



### Available online at www.sciencedirect.com

# **ScienceDirect**

Advances in Space Research 76 (2025) 4815-4837

ADVANCES IN SPACE RESEARCH (a COSPAR publication)

www.elsevier.com/locate/asr

# Spatiotemporal evolution of ecosystem carbon storage under land use/land cover dynamics in the coastal region of Central Vietnam

Viet Hoang Ho a,c,\*, Hidenori Morita b, Thanh Ha Ho c, Felix Bachofer d

<sup>a</sup> Graduate School of Environmental and Life Science, Okayama University, 1 Chome-1-1 Tsushimanaka, Kita Ward, Okayama 700-8530, Japan <sup>b</sup> Graduate School of Environmental, Life, Natural Science and Technology, Okayama University, 1 Chome-1-1 Tsushimanaka, Kita Ward, Okayama 700-8530, Japan

<sup>c</sup> University of Agriculture and Forestry, Hue University, 102 Phung Hung Str, Hue City 53000, Viet Nam <sup>d</sup> German Aerospace Center (DLR), Earth Observation Center, 82234 Wessling, Germany

Received 6 April 2025; received in revised form 12 June 2025; accepted 25 August 2025 Available online 26 August 2025

#### Abstract

Ecosystem carbon storage is a cost-effective strategy for global climate change mitigation, and its fluctuation is markedly shaped by land use/land cover (LULC) dynamics. Taking Danang city as an example of Central Coastal Vietnam, this study aims to assess LULC changes and analyze the spatiotemporal evolution of carbon storage from 2023 to 2050 under four LULC change scenarios, including natural trend scenario (NTS), ecological protection scenario (EPS), economic development scenario (EDS), and cropland protection scenario (CPS), by integrating the support vector machine-cellular automata-Markov (SVM-CA-Markov) model and the InVEST model. The Optimal Parameters-based Geographical Detector (OPGD) model was subsequently employed to elucidate the impacts of driving factors on the spatial distribution of carbon storage. The results showed that, from 2007 to 2023, Danang city experienced a dramatic back-and-forth transformation between LULC types, with the predominant transitions being from natural forest to acacia treedominated plantation forest (6492.31 ha), and from cropland to settlements, acacia tree-dominated plantation forest, and other land (5483.05 ha, 3763.66 ha, 2762.35 ha, respectively). Between 2023 and 2050, LULC transformations in Danang city are projected to yield varying degrees of carbon storage levels across different scenarios. Specifically, carbon storage is anticipated to dwindle by 0.221 Mt, 0.223 Mt, and 0.298 Mt under NTS, EDS, and CPS, respectively, while enhancing by 0.141 Mt under EPS. Regarding the spatial distribution of carbon storage, high values will be chiefly found in the western high-elevation mountainous region, while low values will be concentrated mostly in the eastern lower-lying areas of the city. Additionally, elevation and temperature acted as the two most significant driving factors influencing the spatial distribution of carbon storage, with Q values of 0.88 and 0.86 (p-value < 0.05), respectively. For interaction detection, the combination of elevation and soil exhibited a synergistic reinforcement effect on the spatial partitioning of carbon storage, with a high Q value of 0.9566 (p-value < 0.05). Our study highlights the necessity of ecological conservation measures in Danang city in the on-track pursuit of national net-zero carbon emissions by 2050.

© 2025 The Author(s). Published by Elsevier B.V. on behalf of COSPAR. This is an open access article under the CC BY license (http://creativecommons.org/licenses/by/4.0/).

Keywords: Carbon sequestration; Scenario-based modeling; Remote sensing; Spatial autocorrelation analysis

*E-mail addresses*: hoviethoang@hueuni.edu.vn (V.H. Ho), h-morita@okayama-u.ac.jp (H. Morita), hothanhha@hueuni.edu.vn (T.H. Ho), Felix.Bachofer@dlr.de (F. Bachofer).

# 1. Introduction

Carbon storage in terrestrial ecosystems is a crucial ecological function that contributes to cost-effective strategies for mitigating global climate change (Deng et al., 2017; Singh et al., 2015; Ussiri and Lal, 2017). Nevertheless, land

<sup>\*</sup> Corresponding author at: Graduate School of Environmental and Life Science, Okayama University, 1 Chome-1-1 Tsushimanaka, Kita Ward, Okayama 700-8530, Japan, and University of Agriculture and Forestry, Hue University, 102 Phung Hung Str, Hue City 53000, Viet Nam

use/land cover (LULC) changes driven by human-induced activities such as deforestation, agricultural expansion, and urbanization, have pronouncedly impacted this process both in vegetation and soils, resulting in an escalation in carbon losses through carbon dioxide (CO<sub>2</sub>) emissions and, in turn, exacerbating the challenges of climate change (Houghton et al., 2012; Pielke et al., 2011; Zhu et al., 2022). Specifically, LULC changes are widely recognized as the second most significant anthropogenic source of carbon emissions after fossil fuel combustion (Ussiri and Lal, 2017), with approximately  $1.2 \pm 0.7$  Gt C yr<sup>-1</sup>, accounting for approximately 10.81 % of total annual anthropogenic  $CO_2$ emissions during the 2013-2022 period (Friedlingstein et al., 2023). The CO<sub>2</sub> emissions from LULC changes are typically caused by conversions between LULC types that differ in carbon storage capacities (Schulp et al., 2008; Yan et al., 2024). Generally, forests contain the largest ecosystem carbon content, followed by grassland, arable lands, and other non-forest lands (Corbera et al., 2010; Mauya et al., 2019; Olorunfemi et al., 2020). As a result, converting from land with higher carbon storage leads to a loss of carbon storage, and vice versa (Houghton, 2018; Huang et al., 2023; Nilsson and Schopfhauser, 1995; Ussiri and Lal, 2017). Accordingly, the attempts at spatiotemporally explicit carbon storage evolution from the perspective of LULC structural changes and under various future scenarios have received increasing attention as a valuable strategy to optimize land-based climate change alleviation (Jiang et al., 2022; Kura and Beyene, 2020; Zheng and Zheng, 2023).

As modeling LULC change becomes increasingly critical, numerous land change modelers (LCM) have been created to facilitate the examination of prospective LULC changes and their determinants, as well as to aid in LULC planning and policy formulation (Dezhkam et al., 2016; Nyamekye et al., 2021; Omar et al., 2014). The extant approaches for LCM primarily are empirical and statistical (e.g., Markov chains and regression) models, dynamic models (e.g., cellular automata, agent-based model, and system dynamic), and integrated (e.g., CLUE) models (Guan et al., 2011). Among these, cellular automata (CA) have become the most widely adopted approach due to their efficiency, simplicity, transparency, and capacity to capture the dynamic nature of LULC changes (Kura and Beyene, 2020; Munthali et al., 2020). However, CA emphasizes controlling the spatial pattern of LULC change by considering the configuration of neighboring cells and transition rules which can be detected through an analysis of driving forces (e.g., population density, morphometric data, distance to commercial area, distance to main roads) and calibration algorithms (e.g., multilayer perceptron (MLP), logistic regression, support vector machines (SVM)), rather than controlling the temporal changes among LULC types as a Markov chain process would (Gharaibeh et al., 2020; Ghosh et al., 2017; Guan et al., 2011; Kim, 2010; Mustafa et al., 2018). Thus, integrating the capabilities of the Markov chain and CA represents a robust approach for modeling spatial and temporal variations in LULC change within complex systems (Munthali et al., 2020; Solaimani and Darvishi, 2024), In recent advances, the CA-Markov chain simulation model combined with ecological models e.g., the Integrated Valuation of Ecosystem Services and Trade-offs (InVEST), Century, and Biome-BGC, has emerged as a reliable technique that provides promising results for assessing the impacts of LULC dynamics on ecosystem carbon storage (Verma et al., 2024). The InVEST model with its advantages, including the use of a limited number of parameters, rapid operation, ability to reflect the relationship between LULC change and carbon storage, and capacity to spatially represent the allocation and dynamic variations of carbon storage, has prevalently been utilized (García-Ontivuelo et al., 2024; Yan et al., 2024). More importantly, InVEST is appraised to be successful in evaluating the impacts of diverse policies and planning strategies on regional carbon storage, enabling the balance between overexploitation and conservation (Verma et al., 2024). Existing studies have demonstrated the high utility of linking CA-Markov and InVEST models in assessing the effects of LULC change scenarios on carbon storage (Bacani et al., 2024; Lei et al., 2024; Yan et al., 2024; Zhao et al., 2019).

The coastal zone, which serves as an interface between terrestrial and marine environments (Zhang et al., 2022), possesses several distinctive features. Firstly, coastal areas are among the most rapidly urbanized geographical regions with a high concentration of human activities (Zheng et al., 2020). Secondly, as a considerable carbon reservoir, the coastal region's carbon pool is crucial to the carbon cycle across various spatial scales. That is to say, the alteration of landscape configurations and carbon fixation processes, attributed to the considerable LULC changes in coastal areas, typically results in carbon losses exceeding those of other regions (Zhu et al., 2022). On the one hand, in the context of Vietnamese coastal areas, since the Doi Moi (Renovation, related to the nationwide economic reform) policy in 1986, the influences of globalization have prompted the economy to develop rapidly, making it one of the less developed but rapidly developing regions where human activities and global changes vigorously interact (Liang et al., 2022; M. et al., 2012; Phuong and Richard, 2011; Tuan, 2022). Specifically, in most coastal regions of Vietnam, especially in the Central Coastal area, there has been a continuous and rapid rise in construction land, with its proportion rising from 2.72 % in 2000 to 4.40 % in 2020, converted from either natural landscapes such as forests and grassland or agricultural lands (Liang et al., 2022), thereby contributing the terrestrial carbon losses. On the other hand, according to Kissinger et al. (2021), during the same period (post-1986), Vietnam's terrestrial ecosystem underwent a remarkable turnaround from net loss to net regrowth in forest cover, primarily through conversion from unproductive cultivated land to acacia treedominated plantation forestry and some natural regeneration, expanding from 9.4 million ha in 1990 to 14.8 million

ha by 2015. This growth is ascribed to various ecological engineering policies and state-sponsored programs implemented to promote the conversion of different LULC types to forest lands, thereby improving terrestrial carbon storage. The best examples of these policies/programs are the Forest Land Allocation (FLA) policy (Pham et al., 2023), the Vietnam Forestry Development Strategy 2006–2020 which set a statutory target to boost the total forest cover (including plantations) to 47 % of the national land area in 2020 (V.H. et al., 2020), and the payments for forest ecosystem services (PFES) which represent one alternative and voluntary way to secure financial sources for multifunctional and protective forest (Cochard et al., 2020). These two conflict transition trend patterns (conversion from and to natural landscapes) consequently caused the complex spatial and temporal LULC change in Vietnam's Central Coastal region, leading to uncertainties in estimating terrestrial carbon storage evolution. Therefore, accurately simulating LULC change and unraveling its relationship with ecosystem carbon storage are essential for the stewardship of existing land-based carbon stocks in Central Coastal Vietnam.

The main objectives of this study are: (1) to assess the transitions of LULC from 2007 to 2023, (2) to analyze

the carbon storage evolution under multiple LULC change scenarios from 2023 to 2050, (3) to determine the influential degrees of driving factors on the spatial distribution of carbon storage in the Coastal region of Central Vietnam. The findings in our study are expected to provide reliable references and precise data support for coastal landscape-scale management and decision-making in the research site.

### 2. Materials and methods

### 2.1. Study area

This study was conducted in Danang city (between 15°55′ to 16°13′ North and 107°49′ to 108°20′ East) (Fig. 1), a geographically elongated and narrow region that is recognized as a vibrant urban center within the Key Economic Zone of Central Coastal Vietnam (Hoang Khanh Linh and Van Chuong, 2015). The study area is characterized by topographic heterogeneity, with altitudes being up to 1663 m above sea level and spreading from the delta region in the east to the mountains in the west. As a tropical monsoon climate, the area experiences two distinct annual seasons: a dry period from January to July and a rainy period from August to December (Ho et al., 2024).

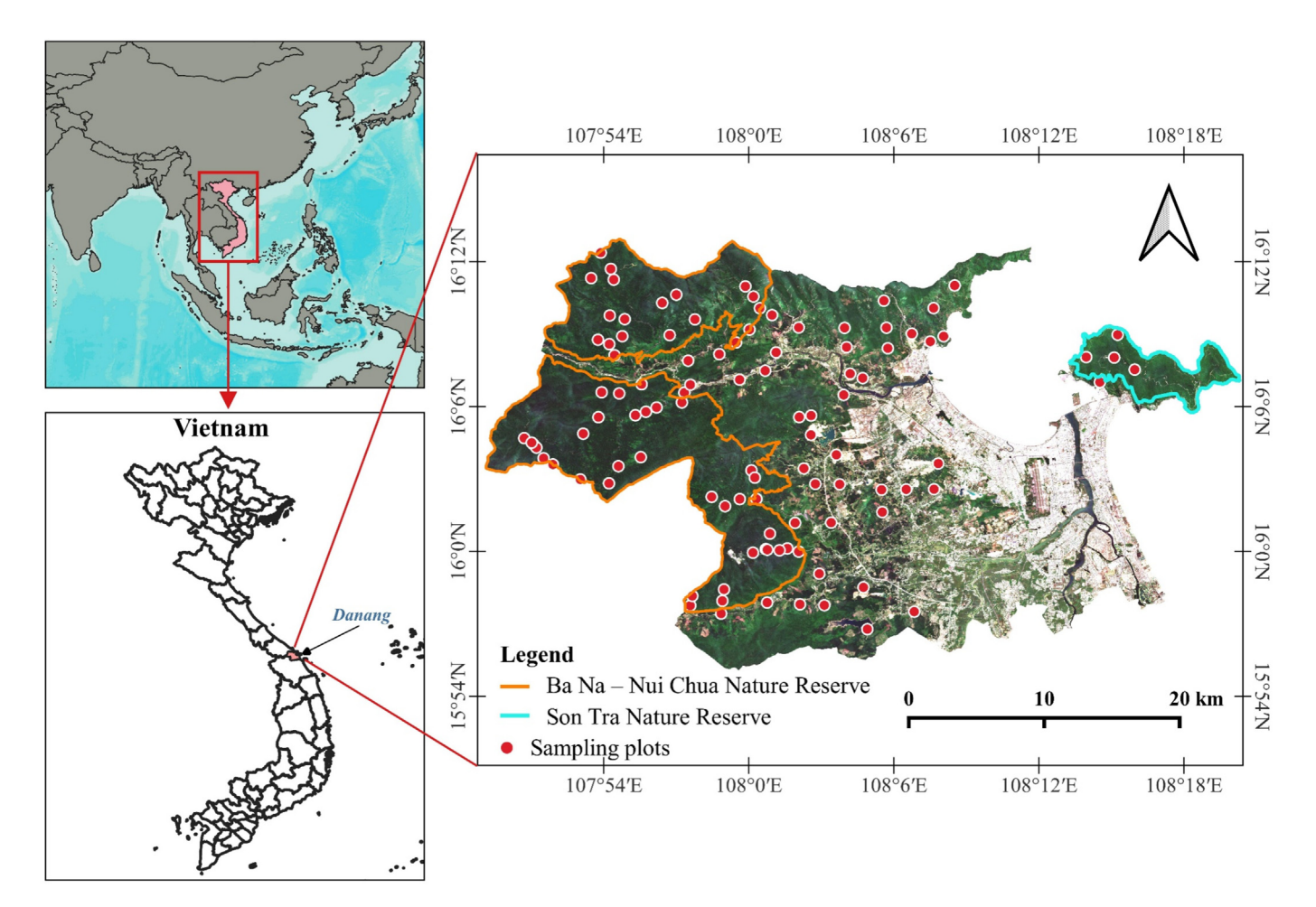


Fig. 1. Location of the study area and sampling plots.

In 2023, the forest area comprised the largest proportion (more than half) of the city's total area. Danang has experienced rapid socioeconomic transformation following the implementation of the *Doi Moi* policy and its administrative separation from Quang Nam Province in 1997, which led to its designation as a centrally governed city. Since then, it has become one of the most densely populated, industrialized, and urbanized centers in Vietnam's Central Coastal region (M. et al., 2012), making it an ideal case for examining the impacts of LULC change on ecosystem services, particularly carbon sequestration.

#### 2.2. Dataset

# 2.2.1. Historical LULC maps

The 10-m resolution LULC map of the study area for 2023 was generated using the random forest classifier based on multi-source remote sensing data (Sentinel-1, Sentinel-2, and Shuttle Radar Topography Mission (SRTM) Digital Elevation Model (DEM) data) in Google Earth Engine (GEE, https://code.earthengine.google.co.in). 427 ground truth points collected in 2023 using a global positioning system (GPS) through field surveys and visual interpretation of high-resolution Google Earth imagery were split into 70 % for training and 30 % for validating the LULC classification. The map legend was based on six IPCC (2006) classes, namely forest, cropland, grassland, wetlands, settlements, and other land. Given the considerable escalation in plantation forest area observed in central Vietnam over the research period (Cochard et al., 2017; Paudyal et al., 2020), we subdivided the forest class into natural forest and plantation forest, using the plantation area delineations obtained from the Danang Department of Forest Protection. The generated 2023 LULC classification map had a satisfactory accuracy, with overall accuracy (OA) and Kappa coefficient (K) exceeding the commonly accepted threshold of 85 % and 0.80, respectively (Nyamekye et al., 2021).

Besides, LULC maps with a 10-m spatial resolution for the study area, covering the years 2007 and 2020, were obtained from the Japan Aerospace Exploration Agency (JAXA, https://www.eorc.jaxa.jp). We subsequently reclassified twelve inherent LULC types in the dataset into seven classes to align with the above 2023 LULC map. The historical LULC maps of the research site are presented in Fig. 5.

# 2.2.2. Driving factors

In this research, the driving factors, including elevation, slope, soil, mean annual precipitation (MAP), mean annual temperature (MAT) distance to main roads (DTR) and distance to rivers (DTW), population density (PD), distance to the central business district area (DTC), and normalized difference vegetation index (NDVI), were derived from various data sources. The details of these driving factors data and their spatial distributions are given in Table 1 and Fig. 2.

All driving force data were then resampled to 10 m spatial resolution to align with the spatial resolution of LULC maps. For LCM, the multicollinearity issue among the driving variables was assessed and determined by absolute Pearson's correlation coefficients (r), with a threshold set at values exceeding 0.80 (Zhi et al., 2021).

# 2.2.3. Carbon density data

In this study, the forest carbon density data of Danang city was calculated using in situ data from a field sample survey in 2023, while the carbon density of other LULC types was obtained by referring to Avitabile et al. (2016) and Dondini et al. (2023). A total of 104 sampling plots were established to collect forest field data using a systematic unaligned sampling design, which combines the spatial regularity of systematic sampling with the randomness of simple random sampling to minimize spatial bias (McRoberts et al., 2015). The procedure for identifying these sampling locations involved two key steps: (1) a 2.5 km × 2.5 km grid was generated based on the forest administrative map provided by the Danang Department of Forest Protection, and (2) within each grid cell, a geographic coordinate was randomly selected using a random point

Table 1 Detailed information on driving factors.

Data type	Data source and processing	Resolution
Elevation	Elevation and slope were extracted from SRTM DEM data in GEE (https://code.earthengine.google.co.in)	30 m
Slope		
MAP	MAP and MAP were downloaded directly from the WorldClim dataset (https://worldclim.org)	1 km
MAT		
DTR	DTR was generated using the road layer from the forest administrative map provided by the Danang Department of Forest	_
	Protection	
DTW	DTW was calculated using SRTM DEM data in GEE (https://code.earthengine.google.co.in)	30 m
PD	PD was obtained from the WorldPop dataset (https://hub.worldpop.org)	1 km
DTC	A field visit identified Hai Chau district as the central business district of the city, notable for its accessibility and high	10 m
	concentration of specialized goods and services compared to other areas. After that, DTC was created using the Hai Chau	
	district's boundary	
NDVI	NDVI was calculated using Sentinel-2 MSI level-2A image collection in GEE (https://code.earthengine.google.co.in)	10 m

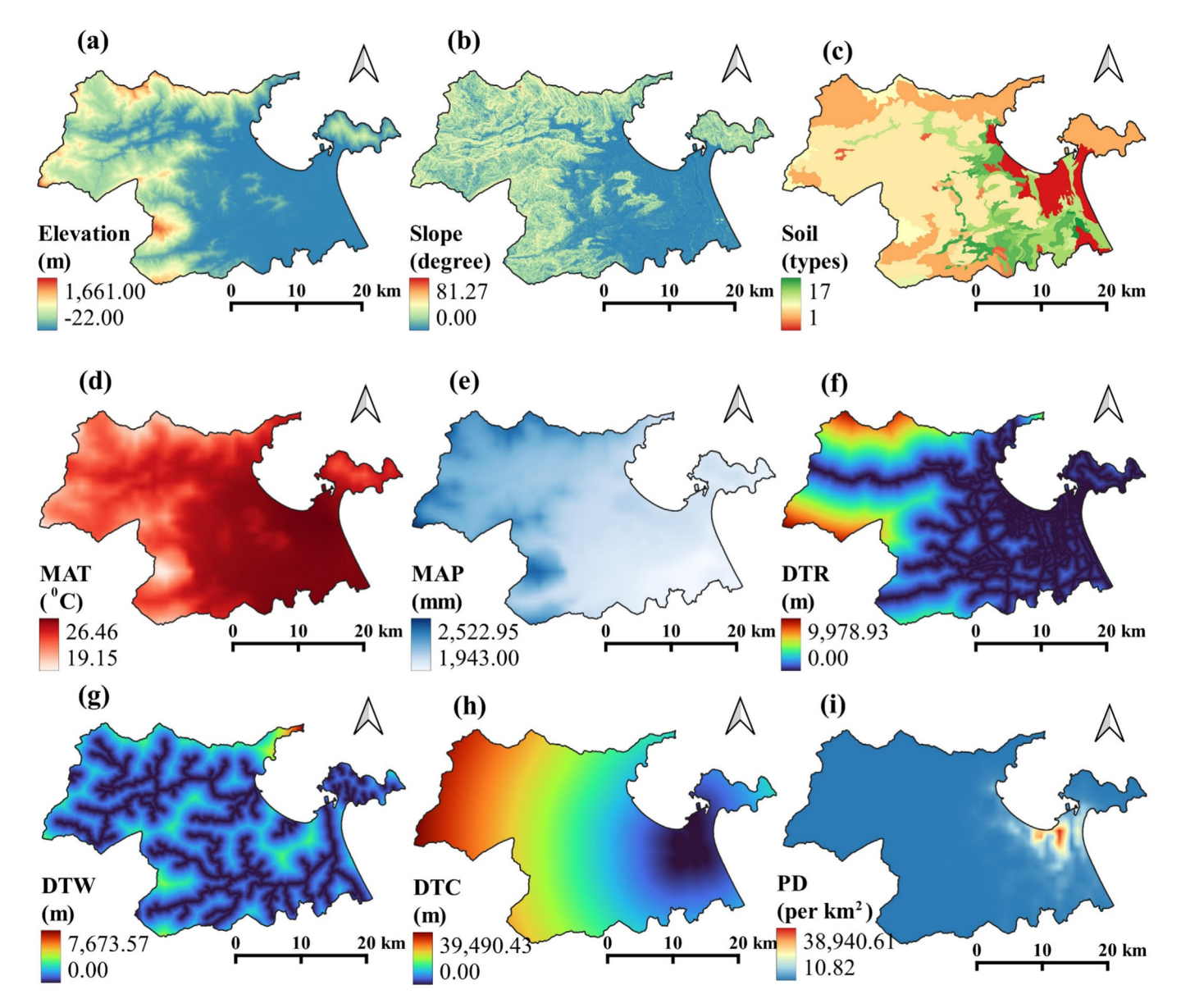


Fig. 2. Spatial distribution of driving forces for LULC change, including elevation (a), slope (b), soil (c), MAT (d), MAP (e), DTR (f), DTW (g), DTC (h), and PD (i).

generator in QGIS. The resulting sampling points were then transferred to portable GPS devices (Garmin GPSMAP 64) and used for navigation during fieldwork. Since carbon storage in forest ecosystems consists mainly of above- and belowground biomass, dead organic matter, and soil organic carbon (Zhu et al., 2022), we designed nested plots (Fig. 3) at designated locations to collect these data. Each plot consisted of a 900-m² main plot with three 1-m² subplots systematically placed along a 14.14-m interval transect, extending from the southwest to the northeast corner of the main plot.

Aboveground biomass encompasses all living vegetation, including trees (diameter at breast height – DBH above 5 cm) and non-tree vegetation (shrubs and herbs). DBH of all trees at 1.3 m above ground was measured

using D-tapes within the main plot, while all shrubs and herbs in the three subplots were cut and weighed directly in the field. Mixed subsamples of herbs and shrubs were then transported to the laboratory to determine moisture content. The carbon stored in dead organic matter was quantified by measuring the aggregation of leaf litter and dead wood biomass. Leaf litter within three subplots was weighed in the field, with evenly mixed subsamples collected for laboratory moisture content analysis. Deadwood (standing and lying) was measured within the same plots as living trees, and its decomposition levels were simultaneously recorded (Level 1 – trees with both branches and twigs, and Level 2 – trees without branches or twigs). For standing dead trees, those at Level 1 were measured similarly to living trees, while Level 2 trees had their height,

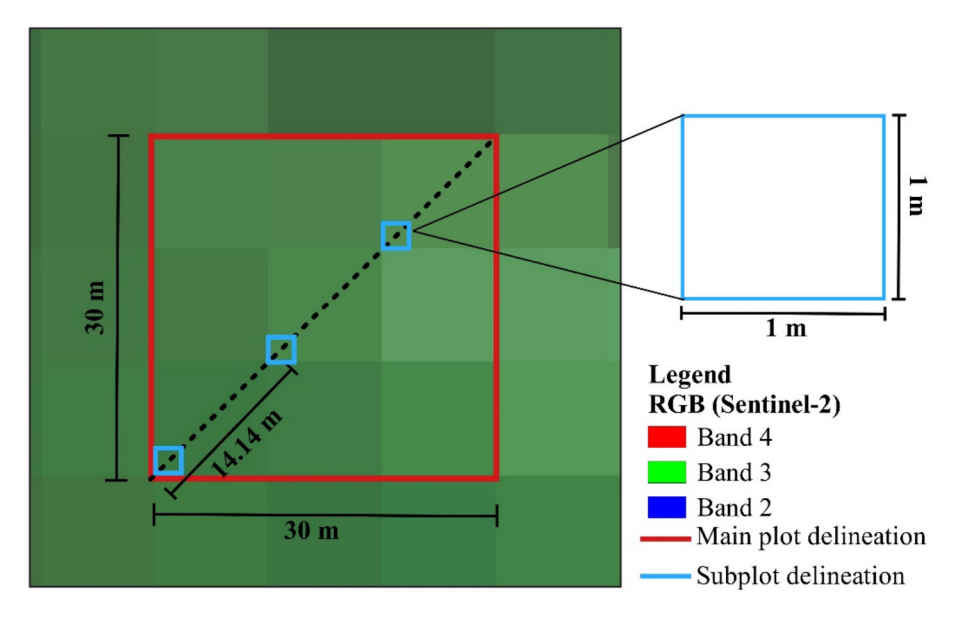


Fig. 3. Sampling plot design for collecting information on carbon pools.

ground-level diameter, and top diameter recorded. Lying deadwood with a DBH above 10 cm was assessed using the line-intersect method, recording diameters and density classes (sound, intermediate, rotten), with representative wood discs collected for each class to determine density. Soil samples of 30 cm depth were collected using soil cores and probes in three subplots, and these samples were subsequently bagged, labeled, and brought to the laboratory for organic carbon analysis.

The procedure for laboratory analysis and calculation of carbon stock density from various pools followed the guidelines of Pearson et al. (2007). Accordingly, subsamples of herbs, shrubs, leaf litter, and wood discs were oven-dried to determine their constant dry weights. Specifically, herbs, shrubs, and leaf litter were dried at 70 °C for 48 h, while wood discs were dried at the same temperature for 72 h. Aboveground biomass density (AGBD) was calculated by aggregating the biomass density of tree (AGBD<sub>tree</sub>), herb (HBD), and shrub (SBD). Among these, AGBD<sub>tree</sub> was calculated using Eq. (1) developed for evergreen broadleaf forests in the South Central Coastal ecoregion of Vietnam by Huy et al. (2016), while HBD and SBD were calculated using Eq. (2).

$$AGBD_{tree}(t.ha^{-1}) = \frac{\sum_{i=1}^{n} 0.104189 \times DBH_{i}^{2.491453}}{A_{mainplot}} \times 10$$
 (1)

where  $DBH_i$  is the diameter at breast height of tree i (cm) and  $A_{mainplot}$  is the main plot area (m<sup>2</sup>).

$$HBD/SBD/LBD(t.ha^{-1}) = \frac{W_{herb/shrub/litter\ field}}{A_{subplots}} \times \left[ \frac{W_{herb/shrub/litter-sample(dry)}}{W_{herb/shrub/litter-sample(fresh)}} \right] \times 10 \tag{2}$$

where  $W_{herb/shrub/litter\,field}$  is the fresh weight of herb/shrub/leaf litter sample in three subplots (kg),  $A_{subplots}$  is the total area of three subplots (m<sup>2</sup>),  $W_{herb/shrub/litter-sample(dry)}$  is the oven-dried weight of herb/shrub/leaf litter sub-sample (g), and  $W_{herb/shrub/litter-sample(fresh)}$  is the fresh weight of herb/shrub/leaf litter sub-sample (g).

Belowground biomass density (BGBD) was estimated using Eq. (3) developed by Cairns et al. (1997) for tropical landscapes.

$$BGBD(t.ha^{-1}) = exp(-1.0587 + 0.8836 \times lnAGBD)$$
 (3)

Biomass of dead organic matter density (DBD) was estimated by the sum of leaf litter biomass density (LBD), standing deadwood biomass density (SDBD), and lying deadwood biomass density (LDBD). LBD, SDBD at the decomposition Level 1, SDBD at the decomposition Level 2, and LDBD were calculated by Eq. (2), Eq. (1), Eq. (4), and Eq. (5), respectively.

$$SDBD(t.ha^{-1}) = \sum_{i}^{n} \left( WD \times \left[ \frac{1}{3} \pi h_i \left( r_{b_i}^2 + r_{t_i}^2 + r_{b_i} \times r_{t_i} \right) \right] \right)$$
(4)

$$LDBD(t.ha^{-1}) = \sum_{i}^{n} \left( WD \times \left[ \pi^{2} \frac{d_{1}^{2} + d_{2}^{2} + \dots + d_{i}^{2}}{8L} \right] \right)$$
 (5)

$$WD(t/m^3) = \frac{mass}{volume} \tag{6}$$

where WD is the wood density for each density class  $(t/m^3)$ , mass is the mass of oven-dried wood disc (t), volume is the volume of the fresh wood disc  $(m^3)$ ,  $h_i$  is the height of deadwood i (m),  $r_{b_i}$  is the radius at the base of deadwood i (cm),  $r_{t_i}$  is the radius at the top of deadwood i (cm),  $d_i$  is diameters of intersecting pieces of deadwood i (cm), and L is the length of line (m).

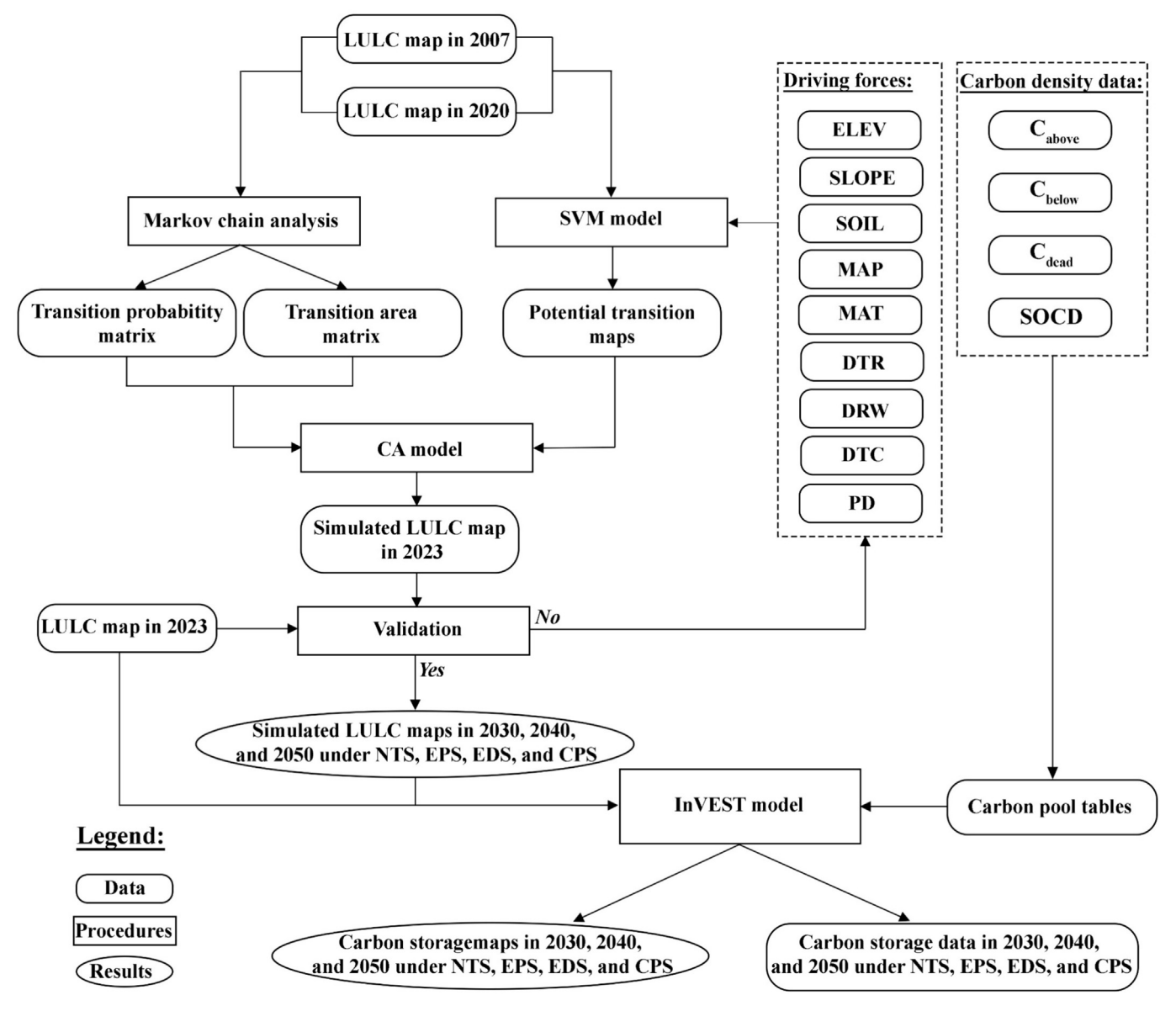


Fig. 4. Flowchart of LULC change and carbon storage modeling.

After that, biomass carbon densities, namely above carbon ( $C_{above}$ ), below carbon ( $C_{below}$ ), and dead carbon ( $C_{dead}$ ), were estimated by applying a conversion factor of 50 % to the respective AGBD, BGBD, and DBD.

Soil organic carbon density (SOCD) was calculated using the following equation:

$$SOCD(t.ha^{-1}) = (SBD \times D \times C) \times 100 \tag{7}$$

where SBD is the soil bulk density of fine fraction (g/cm<sup>3</sup>), D is soil depth (cm), and C is carbon concentration data ( $\frac{9}{2}$ ).

For *SBD* determination, samples from soil cores were dried in an oven at 105 °C for a minimum of 48 h and calculated using Eq. (8). For *C* determination, the materials taken by soil probes were air-dried, sieved through a 2 mm sieve, and thoroughly mixed before being measured by an MT-700 CN CORDER machine (Yanaco, Japan).

$$SBD(g/cm^3) = \frac{ODM}{CV - (\frac{CFM}{DED})}$$
(8)

where ODM is the oven-dry mass of fine fractions (g), CV is the core volume (cm<sup>3</sup>) CFM is coarse fragment mass (g), and RFD is rock fragment density (given as 2.65 g/cm<sup>3</sup>).

# 2.3. Modeling LULC change with SVM-CA-Markov models

In the current study, the SVM-CA-Markov model was proposed for predicting LULC change using the LCM module of TerrSet software. The process was presented in Fig. 4, occurring in three steps: (1) applying Markov chain analysis to 2007 and 2020 LULC maps for computation of transition probabilities and transition areas, (2) using SVM to calibrate 2007–2020 LULC changes with the driving forces to explore the set of rules for LULC transition potentials on a yearly basis by considering the effects of

the neighboring LULC states, and (3) using the CA model to predict the spatial distribution of LULC from the transition probabilities and the transition potential maps.

The Markov chain model, based on empirical statistics, is promising for LULC change modeling as it quantitatively calculates pixel transition probabilities over time using a transition probability matrix, providing a foundation for future predictions (Marko et al., 2016; Subedi et al., 2013; Yan et al., 2024). The formulae for the Markov chain are as follows:

$$S_{t+1} = P_{ij} \times S_t \tag{9}$$

$$P_{ij} = \begin{bmatrix} p_{11} & p_{12} & \cdots & p_{1n} \\ p_{21} & p_{22} & \cdots & p_{2n} \\ \vdots & \vdots & \ddots & \vdots \\ p_{n1} & p_{n2} & \cdots & p_{nn} \end{bmatrix}$$
(10)

where  $S_{t+1}$  and  $S_t$  are the LULC states at moments t+1 and t, respectively;  $P_{ij}$  is the transfer probability matrix; n is the number of LULC classes and  $\sum_{j=1}^{n} P_{ij} = 1$  for each row i.

Generally speaking, Markov alone is not sufficient for LULC change modeling due to the lack of spatial knowledge related to each LULC category, therefore, it is necessary to integrate with the CA model (Ghosh et al., 2017). The CA model is a spatiotemporally discrete dynamical system that effectively simulates LULC changes over time by applying transition rules to generate spatial distributions of LULC states (Lei et al., 2024; Omar et al., 2014; Yan et al., 2024). According to Yang et al. (2008), defining transition rules in the CA model is challenging due to the complex and non-linear nature of LULC dynamics. To effectively address this concern, LCM carries a hybrid approach as it combines the properties of machine learning (e.g., MLP and SVM) with the merits of the CA model (Mustafa et al., 2018; Verma et al., 2024). In this study, we used SVM to couple with the CA model. The main advantage of SVM is its ability to map input data to a higher-dimensional space using a kernel function, optimizing a balance between margin maximization and error tolerance to handle complex nonlinear relationships (Cervantes et al., 2020; Mustafa et al., 2018; Sun, 2014). The future LULC states are defined in the CA model as follows (Verma et al., 2024):

$$S_{t+1} = f(S_t, N, con(.)) \tag{11}$$

where f represents the transition function, N denotes all cells in the Moore neighborhood, and con(.) accounts for constraints and incentives aligned with the development orientations and policies of the study area. In our case study, four LULC change scenarios, namely natural trend scenario (NTS), ecological protection scenario (EPS), economic development scenario (EDS), and cropland protection scenario (CPS), were proposed (Table 2). These scenarios were designed based on the development goals set in the Danang People Committee's Decision No.2609/QD-UBND approving the action plan to respond to climate change in Danang city for the period 2021–2030 and a vision to 2050, and Prime Minister's Decision No.1287/QD-TTg approving Danang city plan for the period 2021–2030 and a vision to 2050.

The simulated 2023 LULC map was compared with the reference 2023 LULC map to validate the SVM-CA-Markov model. Kappa statistics, including  $K_{\rm no}$ ,  $K_{\rm location}$ ,  $K_{\rm strata}$ , and  $K_{\rm standard}$ , were calculated by following the formulas developed by Pontius and Millones (2011) and utilized to assess the model's accuracy in terms of the location and quantity of correctly classified cells. Once these Kappa indices were deemed acceptable (above 0.80) (Kura and Beyene, 2020), the LULC maps for 2030, 2040, and 2050 were further simulated.

# 2.4. Modeling carbon storage with InVEST

This study utilized the InVEST model to estimate the spatial and temporal distribution of carbon storage in Danang city from 2023 to 2050. The model required three key inputs: the 2023 LULC map, the projected LULC maps generated through LCM, and a carbon pool table containing data from four primary carbon pools. The mathematical representation of calculating carbon storage  $(C_{storage})$  is detailed as follows (Yan et al., 2024):

Table 2
Future scenarios of LULC change for Danang city.

Scenarios	Description
NTS	Under NTS, the demand for LULC is assumed to remain unconstrained and continue following the existing trend evolution observed during the 2007–2020 period.
EPS	The study site includes two ecologically protected areas, Ba Na – Nui Chua Nature Reserve and Son Tra Nature Reserve (Fig. 1). Under
	EPS, an absolute constraint is imposed to prevent the conversion of natural forest within these reserves. Additionally, the probability of
	natural forest outside the reserves being converted to other LULC types is reduced by 40 %. Likewise, the probability of plantation forest being converted to other LULC types is reduced by 40 % (except natural forest).
EDS	Under EDS, the probability of land conversion from other LULC types to settlements is assumed to be augmented by 20 %
CPS	Under CPS, the probability of cropland converting to settlements is assumed to diminish by 70 %, while its conversion to other LULC types
	is reduced by 40 %

$$C_{storage} = \sum_{i=1}^{n} (C_{above,i} + C_{below,i} + C_{dead,i} + SOCD_i) \times S_i$$
(12)

where i is a given LULC type, n is the number of LULC types and equals seven in this study, and  $S_i$  refers to the area of LULC type i.

# 2.5. Optimal parameters-based geographical detector model and spatial autocorrelation analysis

Optimal Parameters-based Geographical Detector (OPGD) model was chosen to quantitatively analyze the effects of the seven driving factors (including elevation, slope, soil, MAT, MAP, PD, and NDVI) and the interactions between these factors in the spatial differentiation of carbon storage through measuring Q value (Song et al., 2020). The study area was divided into a  $300 \times 300$  m grid. and the average values of carbon storage and driving factors extracted within grid cells were used as input data for implementing OPGD in the GD package in the R environment. For optimal spatial data discretization, we applied grid-search to pinpoint the best combination of parameters, including spatial data discretization method (including equal interval, geometrical interval, natural breaks, quantile), and break number of spatial strata (ranging from 3 to 7).

In this study, global Moran's I and LISA local Moran's I were employed for spatial autocorrelation analysis (Anselin, 1995), and both indices were calculated in the

Spdep package in the R environment. Among these, the global Moran's I values ranging from -1 to 1 were used to reflect the overall distribution characteristics of carbon storage. The LISA local Moran's I was subsequently used to identify statistically hot spots, cold spots, and spatial outliers of carbon storage through five quadrants, namely High-High Cluster, High-Low Cluster, Low-High Cluster, Low-Low Cluster, and Not Significant.

### 3. Results

# 3.1. Carbon density calculation

The carbon density varied considerably across different LULC types and carbon pools (Table 3). Natural forest exhibited the highest carbon density (236.45 t.ha<sup>-1</sup>), with biomass carbon being considerably greater than soil carbon (131.00 and 105.45 t.ha<sup>-1</sup>, respectively). Compared to natural forest, plantation forest store approximately half the carbon density (129.81 t.ha<sup>-1</sup>), with the soil carbon pool contributing the largest share (76.07 t.ha<sup>-1</sup>). Both grassland and cropland showed moderate carbon density (60.80 and 46.40 t.ha<sup>-1</sup>, respectively), likely due to their agricultural characteristics. Similar to plantation forest, the majority of carbon in these LULC types was concentrated in the soil carbon pool (53.00 and 40.80 t.ha<sup>-1</sup>, respectively). Whereas, in wetlands, settlements, and other land categories, where vegetation is largely absent, carbon density had the least figures among LULC types and came radically from the soil carbon pool with the same value of 43.20 t.ha<sup>-1</sup>.

Table 3 Carbon density of various LULC types in Danang city.

LULC types	Carbon density (t.ha <sup>-1</sup> )					Source
	Cabove	$C_{below}$	$C_{dead}$	SOCD	Total C	
Natural forest	104.94	19.54	6.52	105.45	236.45	Field data
Plantation forest	42.12	8.72	2.90	76.07	129.81	Field data
Cropland	4.00	1.00	0.60	40.80	46.40	Avitabile et al. (2016)
Grassland	6.50	1.30	0.00	53.00	60.80	Avitabile et al. (2016) and Dondini et al. (2023)
No vegetation (wetlands, settlements, and other land)	0.00	0.00	0.00	43.20	43.20	Avitabile et al. (2016)

Table 4 Changes in LULC types in Danang city from 2007 to 2023.

LULC ty	pes	Natural forest	Plantation forest	Cropland	Grassland	Wetlands	Settlements	Other land
2007	Area (ha)	51546.07	11094.83	22485.94	0.00	2183.88	8745.39	1809.17
	Proportion (%)	52.67	11.34	22.98	0.00	2.23	8.94	1.84
2020	Area (ha)	49284.83	17657.67	9608.31	77.20	2641.13	14720.26	3875.88
	Proportion (%)	50.36	18.04	9.82	0.08	2.70	15.04	3.96
2023	Area (ha)	46319.38	18706.71	10497.44	74.11	1900.17	15007.29	5360.18
	Proportion (%)	47.33	19.11	10.73	0.08	1.94	15.33	5.48
Area change from 2007 to 2023 (ha)		-5226.69	7611.88	-11988.50	74.11	-283.71	6261.90	3551.01

### 3.2. Historical LULC changes

Table 4 demonstrates the total area covered by each LULC class, along with the corresponding percentage and changes (gain/loss) from 2007 to 2023. The results showed that natural forest consistently remained the dominant LULC type in Danang city, occupying nearly half of the total area, with a coverage of 52.67 % in 2007, 50.36 % in 2020, and 47.33 % in 2023. Furthermore, remarkable increases were recorded in plantation forest (7611.88 ha), settlements (6261.90 ha), and other land (3551.01 ha). Whereas, the opposite was true for cropland and natural forest when these LULC types dropped by 11988.50 ha and 5226.69 ha, respectively. Unlike the mentioned LULC type above, the area changes of wetlands and grassland were marginal, solely with 283.71 ha and 74.11 ha, respectively.

According to the historical LULC maps and diagram presented in Fig. 5, Danang city experienced substantial LULC transformations from 2007 to 2023. The loss of cropland was the largest during the 16-year period, reaching nearly half of its total area with 12998.74 ha. Specifically, 5483.05 ha, 3763.66 ha, 2762.35 ha, 605.73 ha, 344.65 ha, and 39.30 ha of cropland were transferred into settlements, plantation forest, other land, natural forest, wetlands, and grassland, respectively. Natural forest possessed the second largest roll-out region of 7027.87 ha, with 6492.31 ha, 448.93 ha, 47.95 ha, 27.04 ha, 9.87, and 1.77 ha of land being transferred into plantation forest, other land, settlements, cropland, grassland, and wetlands, respectively. The total shrinking area of wetlands was 696.70 ha, mainly converted into other land, cropland, and settlements. From a roll-in perspective, plantation forest had the largest transfer area over the past 16 years from 2007, which was 10384.93 ha, primarily sourced from natural forest and cropland, covering 6492.31 ha and 3763.66 ha, respectively. Settlements also had a large expansion area of 6661.98 ha, but its main source solely came from cropland with 5483.05 ha. In addition, other land was steadily accumulated during this period as its area continuously went up, mostly converting from cropland (2762.35 ha) and plantation forest (1027.85 ha).

# 3.3. LULC change modeling

In this study, to avoid the effects of multicollinearity issues on spatial prediction of LULC changes, we carried out a variable selection procedure in the following two steps. Firstly, SVM using nine driving variables, as shown in Fig. 2, was implemented to discover the influence order based on skill measures. Secondly, r values were calculated, and each set of highly correlated variables (r > 0.8) was simplified by removing one variable that had a lower level of influence among the correlated variables. As a result, MAT and MAP were eliminated since they were highly correlated with elevation (0.95 and 0.86, respectively), and elevation had a stronger influence on LULC changes.

Therefore, seven driving variables (elevation, slope, soil, DTR, DTW, DTC, and PD) were retained for LCM. Nine major transition sub-models, as shown in Fig. 6, were integrated with selected driving factors for the calibration process of SVM-CA to establish transition rules. The Markov chain model was employed to capture LULC transitions by evaluating gains, losses, and persistence over 13-year intervals from 2007, generating both the transition probability matrix and the transition area matrix. Future LULC scenarios were then simulated by incorporating SVM-CA and Markov. The simulated validation for assessing the functionality, acceptance, and reliability of the prediction was conducted to examine the effectiveness of the SVM-CA-Markov model by comparing simulated and reference LULC maps of 2023. The accuracy results of the simulated LULC map in 2023 are presented in Table 5. Among the seven LULC types, natural forest, plantation forest, grassland, and settlements showed high agreement, with accuracy ranging from 93.94 % to 96.35 %, indicating that these types in the simulated LULC map closely correspond to the reference LULC map. However, the simulated map shows that natural forest, grassland, and settlements were overestimated by 6.45 %, 4.17 %, and 5.36 %, respectively, while plantation forest was underestimated by 3.65 %. On the other hand, results from cropland, wetlands, and other land showed a lower agreement with accuracies ranging from 69.30 % to 76.48 %, suggesting moderate misclassification between these and other LULC types.

Apart from determining the prediction accuracy of the model through a comparison of reference and simulated LULC maps of 2023, an attempt was made to examine its accuracy with the kappa coefficients (Table 6). The computed kappa coefficients ( $K_{no}=0.9276,\,K_{location}=0.9408,\,K_{strata}=0.9408,\,$  and  $K_{standard}=0.9072$ ), were all above the acceptable threshold of 0.8, implying the SVM-CA-Markov model can effectively predict future LULC in the study area.

Following the validation of satisfactory simulation accuracy, the SVM-CA-Markov model was adopted to project the spatial distribution of LULC in Danang city from 2023 to 2050 under four distinct scenarios, as illustrated in Fig. 6. In general, the simulated spatiotemporal dynamics of LULC types exhibit significant heterogeneity across the four scenarios. Furthermore, these transformations will be predominantly concentrated in the central section (mainly the transition between natural forest and plantation forest, and between cropland and plantation forest) and lower sections (mainly the transition to settlements from other LULC classes) of the research site.

The simulation results in Fig. 7 demonstrate that Danang city's overall LULC patterns will undergo noticeable changes across the four scenarios, with the exception of grassland, which will remain largely unchanged. From 2023 to 2050, NTS will maintain the LULC transition trends and development trajectories observed in the preceding phase, with change magnitudes remaining relatively consistent. The most pronounced expansion will be

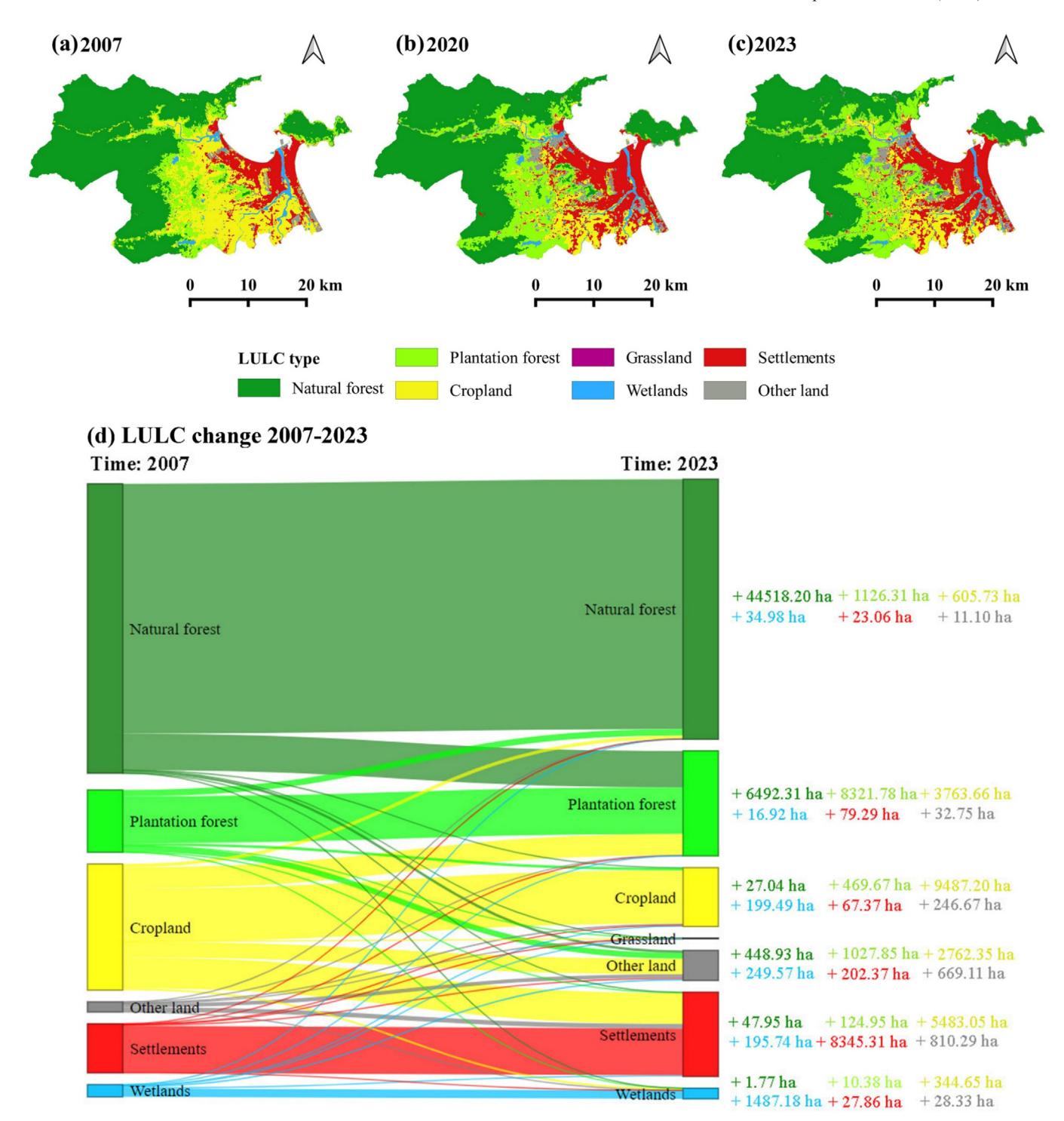


Fig. 5. Spatiotemporal distributions of LULC types in 2007 (a), 2020 (b), and 2023 (c); and Sankey diagram of LULC transformation during 2007–2023 (d).

observed in settlements, increasing by a total of 5116.68 ha, and it will be followed by plantation forest and wetlands with 2459.67 ha and 341.09 ha, respectively. Conversely, cropland, natural forest, and other land will have their areas declined by the respective amount of 5368.01 ha, 2156.12 ha, and 393.31 ha in the same research period. Under EPS, this scenario will impose

constraints to limit the uncontrolled conversion of ecologically significant land, leading to enhanced conservation of natural forests within the nature reserves (Ba Na – Nui Chua and Son Tra) and a slight expansion of both natural and plantation forests outside these protected areas, with 559.47 ha and 586.36 ha, respectively, in the next 27 years. In contrast, EDS, which prioritized economic develop-

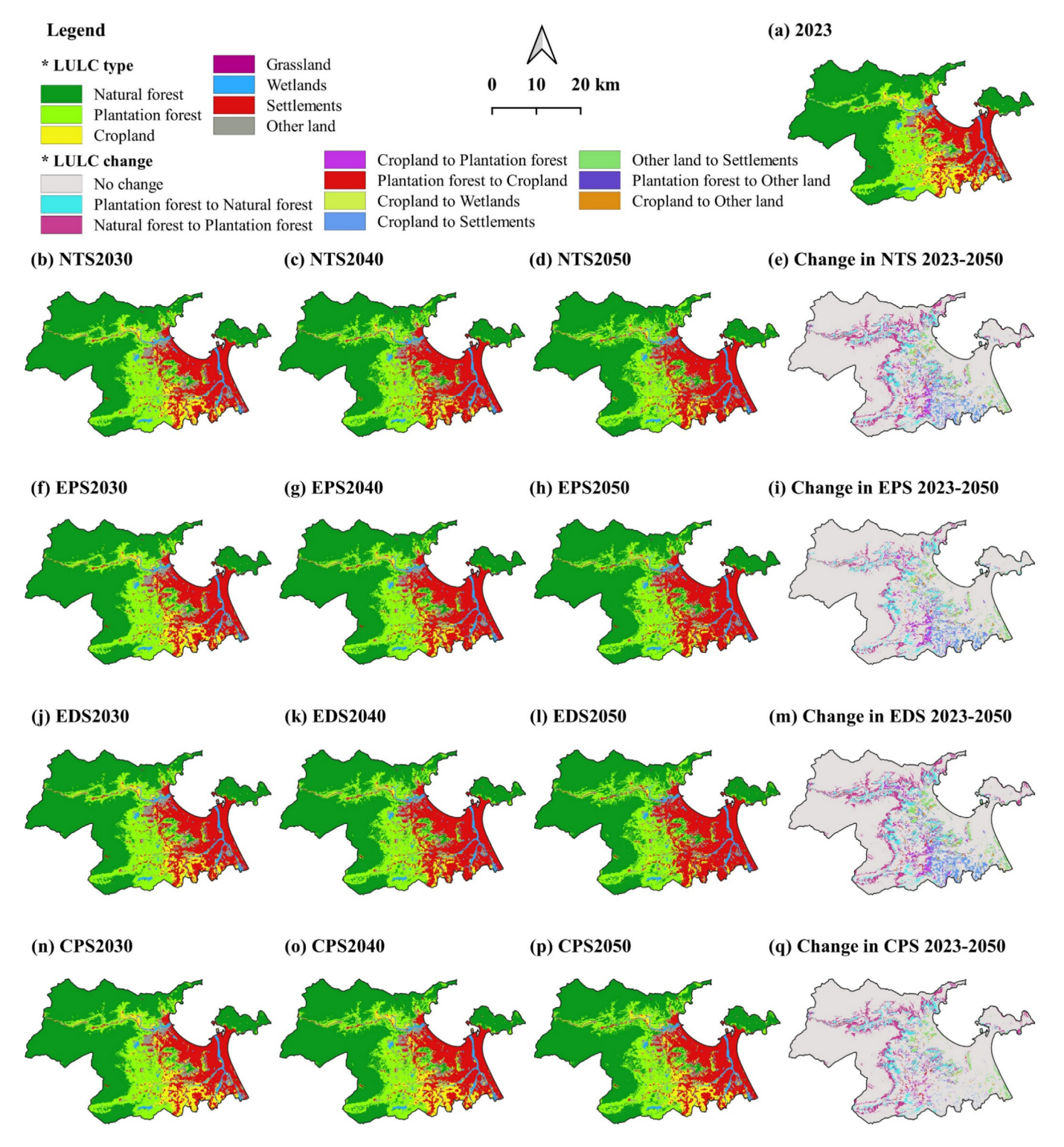


Fig. 6. Spatiotemporal distributions of LULC types and their changes under multiple scenarios in Danang city from 2023 to 2050.

ment, will accelerate LULC transitions toward settlements, resulting in the most extensive expansion of settlement areas among all scenarios. Specifically, the elevated area of settlements in EDS is set to 6358.61 ha, meanwhile, these in NTS and EPS are projected to be the same

by 5116.68 ha, and that in CPS is expected by 2518.59 ha. Notably, CPS will exhibit the smallest reduction in cropland area among the four scenarios, with a shrinkage of only 1205.69 ha, thereby ensuring a more stable level of food security.

Table 5
Accuracy results of the simulated 2023 LULC map.

LULC type	2023 LULC Reference (ha)	2023 LULC Simulated (ha)	Difference(ha)	Difference (%)	Accuracy(%)
Natural forest	46319.38	49306.05	-2986.67	-6.45	93.94
Plantation forest	18706.71	18024.74	681.97	3.65	96.35
Cropland	10497.44	8028.73	2468.71	23.52	76.48
Grassland	74.11	77.20	-3.09	-4.17	96.00
Wetlands	1900.17	2742.02	-841.85	-44.30	69.30
Settlements	15007.29	15810.95	-803.66	-5.36	94.92
Other land	5360.18	3875.59	1484.59	27.70	72.30
Total	97865.28	97865.28	0.00		

Table 6 Validation metrics of the simulated 2023 LULC map.

Information Allocation	Information of Quantity						
	No[n]	Medium[m]	Perfect[p]				
Perfect [P(x)]	P(n) = 0.5212	P(m) = 0.9756	P(p) = 1.0000				
Perfect Stratum $[K(x)]$	K(n) = 0.5212	K(m) = 0.9756	K(p) = 1.0000				
Medium Grid $[M(x)]$	M(n) = 0.4823	M(m) = 0.9367	M(p) = 0.9233				
Medium Stratum $[H(x)]$	H(n) = 0.1250	H(m) = 0.3175	H(p) = 0.3146				
No $[N(x)]$	N(n) = 0.1250	N(m) = 0.3175	N(p) = 0.3146				
Agreement Chance $= 0.1250$							
Agreement Quantity $= 0.1925$							
Agreement Strata $= 0.0000$							
Agreement Grid $cell = 0.6192$							
Disagree Grid $cell = 0.0389$							
Disagree Strata $= 0.0000$							
Disagree Quantity $= 0.0244$							
$K_{\rm no} = 0.9276$							
$K_{location} = 0.9408$							
$K_{\text{strata}} = 0.9408$							
$K_{standard} = 0.9072$							

# 3.4. Carbon storage change modeling

The results from the InVEST model (Fig. 9) illustrate varying degrees of change in carbon storage and density across Danang city under four simulated scenarios from 2023 to 2050. Generally speaking, both carbon storage and density are projected to dwindle in most scenarios, except for EPS. Besides, CPS is anticipated to yield the most substantial decrease in carbon storage, while NTS and EPS show a relatively similar pattern in trend and pace. By 2050, the study area is expected to retain carbon storage within the range of 14.990–15.429 Mt, with carbon density varying between 153.17 and 157.66 t.ha<sup>-1</sup>. Relative to 2023, Danang city's carbon storage by 2050 is forecast to reduce by 0.221 Mt under NTS, 0.223 Mt under EDS, and 0.298 Mt under CPS, while enhancing by 0.141 Mt under EPS. Similarly, the carbon density by 2050 is anticipated to drop by 2.26 t.ha<sup>-1</sup> in NTS, 2.28 t.ha<sup>-1</sup> in EDS, and 3.05 t.ha<sup>-1</sup> in CPS, whereas EPS is expected to exhibit a slight increase of 1.44 t.ha<sup>-1</sup>.

According to the spatial differentiation of carbon storage from 2023 to 2050 shown in Fig. 8, carbon loss and car-

bon sequestration regions will take place in line with LULC change areas. To uncover the spatial agglomeration characteristics of carbon storage in Danang city in 2050 across four scenarios, we adopted the spatial autocorrelation analysis. Under NTS, EPS, EDS, and CPS, the global Moran's I values of carbon storage were 0.939, 0.942, 0.939, and 0.940, respectively (all p-values < 0.05), indicating the existence of strong spatial clustering overall. The LISA Local Moran's I result of cluster and outlier analysis (Fig. 10) show that the spatial distributions of carbon storage under four scenarios will have relative resemblance. Specifically, carbon storage presents a high – not significant – low spatial distribution pattern from west to east. Hot spots (High-High Cluster) will be primarily concentrated in the western parts of Danang city, corresponding to the distribution of undisturbed natural forests in highaltitude mountainous areas. Whereas, cold spots (Low-Low Cluster) will be predominantly found in settlements in the eastern regions of the study area. Furthermore, the number of hot spots will be moderately more than its counterpart in all scenarios, and EPS will emerge subtly more hot spots than in other scenarios.

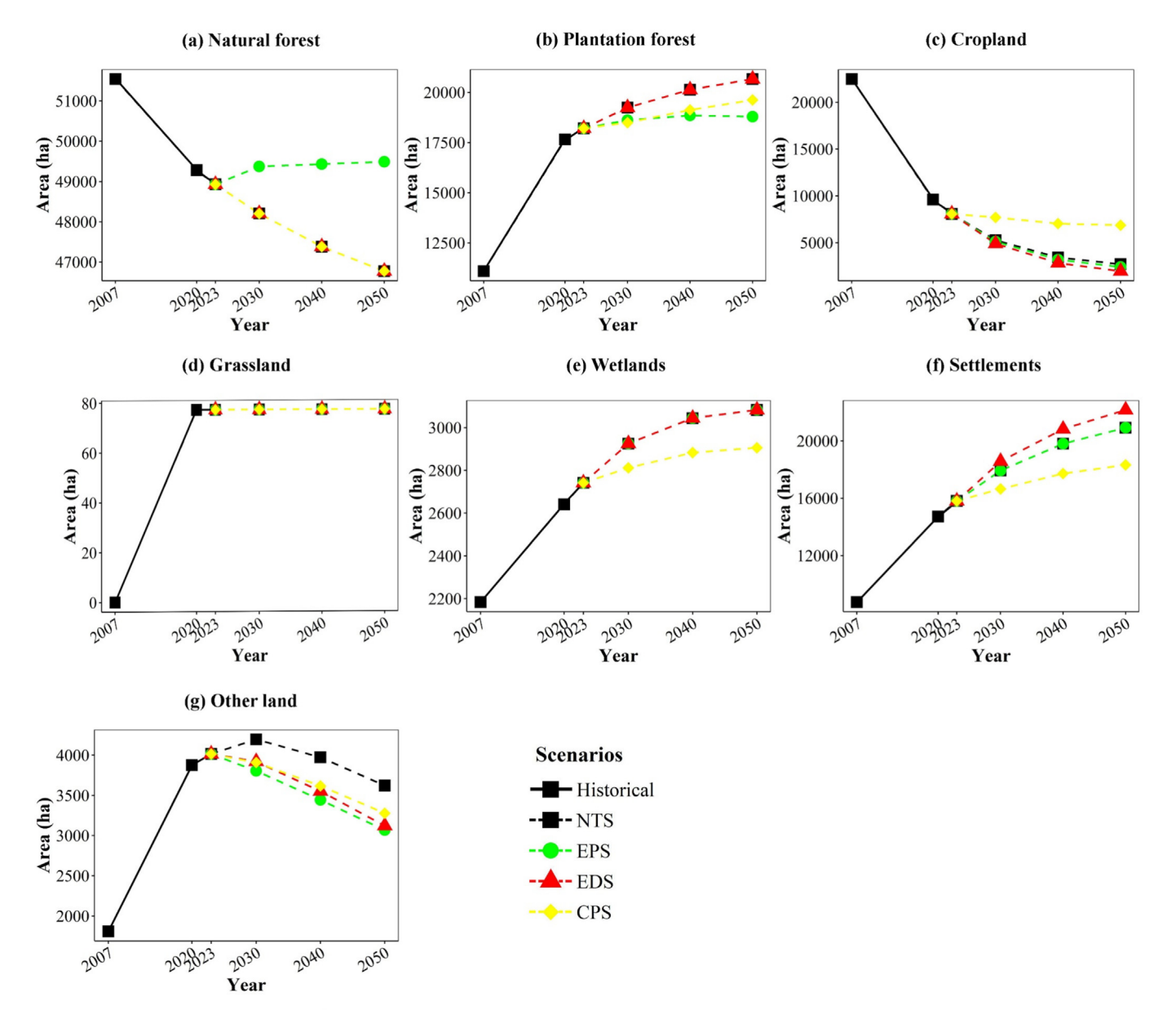


Fig. 7. Changes in LULC types under multiple scenarios in Danang city from 2023 to 2050.

The results in Table 7 show that irrespective of projected years and LULC simulation scenarios, natural forest will be the dominant LULC type within Danang city, accounting for more than 70 % of total carbon storage, and the LULC type that will contribute most to the changes in carbon storage over time. Considering changes in carbon storage across various LULC types, variations will arise due to LULC transitions. However, such carbon storage changes for each LULC type will differ across scenarios, and the overall tendency will conform to the changes in the LULC type of corresponding scenarios. Specifically, the carbon storage in natural forest and cropland will remarkably reduce from 2023 to 2050 in NTS, by 0.510 Mt and 0.249 Mt, respectively, while plantation

forest and settlements reveal a pronounced rise of 0.319 Mt and 0.221 Mt, respectively. Under EPS, while cropland, plantation forest, and settlements will possess the same change pattern as NTS, the carbon storage of natural forest is set to accumulate by 0.132 Mt, indicating that the adoption of ecological protection measurements will partly contribute to achieving a degree of carbon sequestration. Whereas, the amount of sequestered carbon in settlements is forecast to climb the most under EDS (0.275 Mt), and the carbon loss from cropland will be mitigated most effectively under CPS (0.056 Mt), compared to other scenarios. Notably, carbon storage changes in grassland, wetlands, and other land will not be obvious in the four mentioned scenarios by 2050.

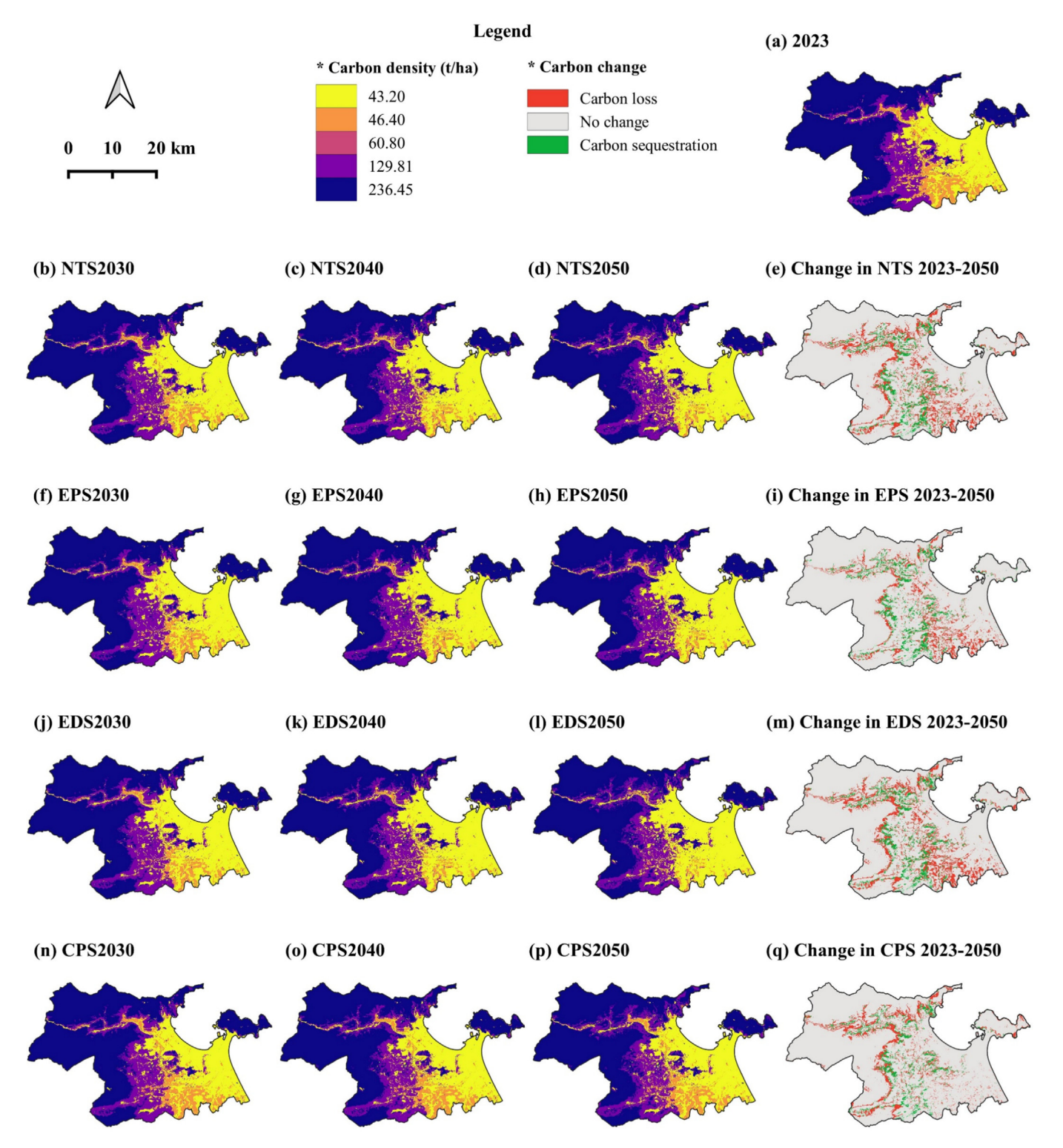


Fig. 8. Spatiotemporal distributions of carbon storage and its changes under multiple scenarios in Danang city from 2023 to 2050.

# 3.5. Analysis of the effects of spatial distribution driving forces on carbon storage

In this study, the OPGD model was performed to explore the potential driving factors (including elevation, slope, soil, MAT, MAP, PD, and NDVI) affecting the spatial distribution of carbon storage in Danang city. Fig. 11

shows the result of the optimal discretization process, and the parameter combinations with the largest Q value were chosen. As a result, the quantile method was chosen to discretize elevation, MAT, and NDVI into seven intervals, and to discretize MAP and PD into six intervals, meanwhile, slope and soil were discretized into six intervals using the standard deviation method.

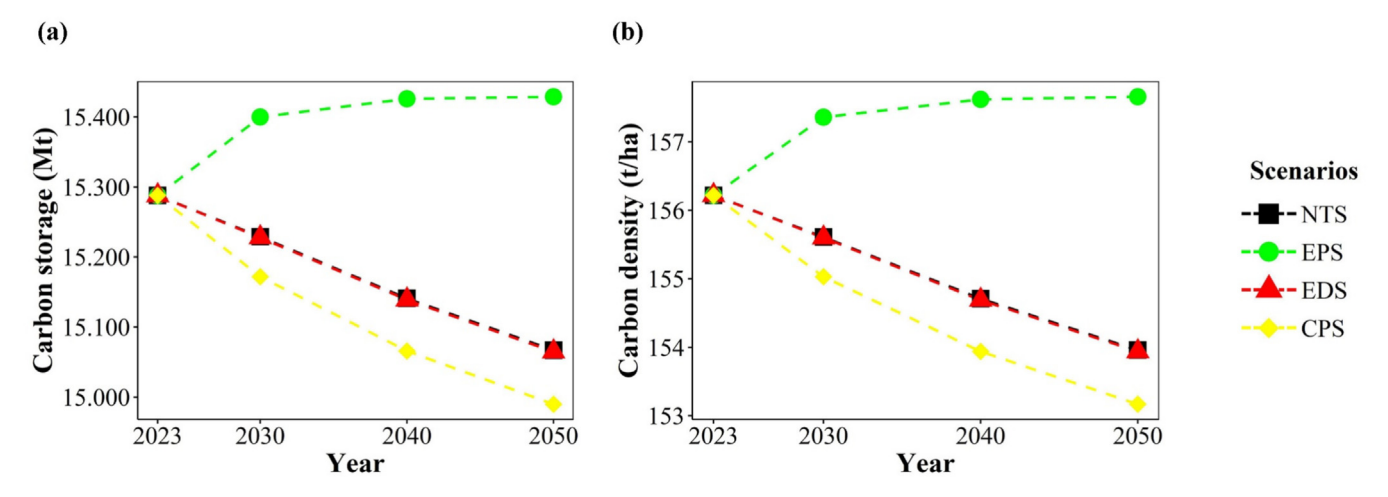


Fig. 9. Changing storage (a) and density (b) of carbon under multiple scenarios in Danang city from 2023 to 2050.

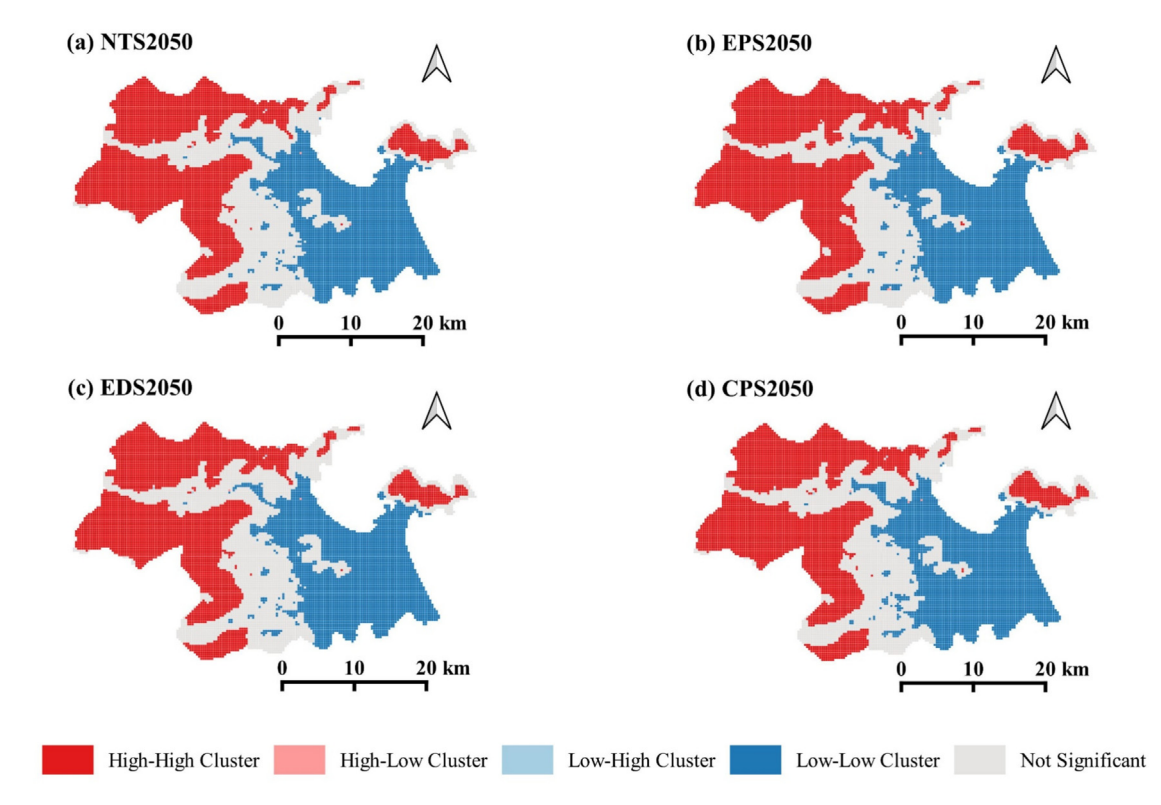


Fig. 10. Local spatial autocorrelation analysis of carbon storage in Danang city under NTS (a), EPS (b), EDS (c), and CPS (d) by 2050.

The results from the single-factor analysis demonstrate that all driving factors significantly influenced the spatial distribution characteristics of carbon storage in the study area (all p-values < 0.05). Fig. 12a illustrates the influencing ranking of driving factors individually in explaining the spatial differentiation of carbon storage. As can be seen, the explanatory power of elevation was the strongest among the driving factors, with a Q value of 0.88. This was followed by MAT (Q value = 0.86), NDVI (Q value = 0.83), slope (Q value = 0.78), PD (Q value = 0.68), and MAP (Q value = 0.64). Soil had the smallest drive, with a Q value

of 0.59. According to the interaction factor analysis (Fig. 12b), the spatial features in carbon storage in Danang city were not merely affected by individual factors, but rather shaped by the cumulative impact of dual-factor interactions. In addition, most of the combined effects of the two factors were unable to enhance the explanatory capability compared to their individual effects, with the exception of the synergy between elevation and soil. Thus, with a high value of 0.9566, the combination of elevation and soil provided a robust interactive explanatory power for the spatial differentiation of carbon storage in the study area.

Table 7 Change in carbon storage of different LULC types in Danang city from 2023 to 2050 (Mt).

Year	LULC type								
	Natural forest	Plantation forest	Cropland	Grassland	Wetlands	Settlements	Other land		
2023	11.570	2.364	0.375	0.005	0.118	0.683	0.173		
NTS2030	11.399	2.498	0.245	0.005	0.126	0.775	0.181		
EPS2030	11.675	2.417	0.238	0.005	0.126	0.775	0.164		
EDS2030	11.399	2.498	0.228	0.005	0.126	0.803	0.169		
CPS2030	11.399	2.401	0.358	0.005	0.121	0.719	0.169		
NTS2040	11.204	2.614	0.160	0.005	0.132	0.856	0.172		
EPS2040	11.689	2.448	0.148	0.005	0.132	0.856	0.149		
EDS2040	11.204	2.614	0.132	0.005	0.132	0.900	0.153		
CPS2040	11.204	2.483	0.327	0.005	0.125	0.766	0.156		
NTS2050	11.060	2.683	0.126	0.005	0.133	0.904	0.156		
EPS2050	11.702	2.440	0.112	0.005	0.133	0.904	0.133		
EDS2050	11.060	2.683	0.091	0.005	0.133	0.958	0.135		
CPS2050	11.060	2.548	0.319	0.005	0.126	0.792	0.142		
Change in NTS 2023-2050	-0.510	0.319	-0.249	0.000	0.015	0.221	-0.017		
Change in EPS 2023–2050	0.132	0.076	-0.263	0.000	0.015	0.221	-0.041		
Change in EDS 2023–2050	-0.510	0.319	-0.284	0.000	0.015	0.275	-0.039		
Change in CPS 2023–2050	-0.510	0.184	-0.056	0.000	0.007	0.109	-0.032		

### 4. Discussion

4.1. Analyzing the historical LULC change and its impacts on carbon storage

Maintaining carbon storage in terrestrial ecosystems has been a long-standing area of interest, as it is essential for elucidating the carbon cycle dynamics and developing effective policies to mitigate emissions (Ismail and Gaganis, 2024; Lei et al., 2024). Nevertheless, dramatic LULC changes induced by anthropogenic factors have remarkably transformed landscape patterns and terrestrial carbon sequestration in vegetation and soil, consequently leading to fluctuations in ecosystem carbon storage (Yan et al., 2024). Previous research indicates that the effect of LULC change on ecosystem carbon storage is primarily determined by the carbon sequestration potential of different LULC types and the patterns of land conversion (Zhu et al., 2022). That is to say, carbon storage tends to accumulate when LULC types with low carbon density are converted to those with higher carbon density, and vice versa (Houghton, 2018; Huang et al., 2023; Nilsson and Schopfhauser, 1995; Ussiri and Lal, 2017). Therefore, analyzing the association between LULC changes and carbon storage can effectively track its evolution (Nayak and Mandal, 2019; Yan et al., 2024). Fig. 5 demonstrates that in the period between 2007 and 2023, Danang city witnessed dramatic back-and-forth LULC changes, with predominant transitions from natural forest to plantation forest (6492.31 ha) and from cropland to settlements, plantation forest, and other land (5483.05, 3763.66, and 2762.35 ha, respectively). Among these, only the transition from cropland to plantation forest resulted in carbon sequestration in Danang city, whereas all other transitions led to carbon loss, given the ranking order of carbon storage capacity from high to low: natural forest, plantation forest, cropland, and non-vegetation (settlements and other land) as shown in Table 3. Consequently, a marked decline in carbon storage was ineluctable in Danang city over the course of 16 years. Moreover, plantation forest experienced the greatest increase in land area, primarily at the expense of natural forest (6492.31 ha) and cropland (3763.66 ha). These LULC conversions were driven by two factors. First, economic modernization, including agricultural intensification on the productive lands, industrialization, and urbanization, resulted in the abandonment of less productive farmlands, which then reverted to plantation forestry (Cochard et al., 2017). Second, the scarcity of forests catalyzed a socio-political transition toward enhanced investment in forest conservation and regeneration, largely through forest policies and government-sponsored initiatives promoting monoculture plantations of non-native species (Cochard et al., 2017). The key policy initiatives included (i) FLA policy accelerated the conversion from natural forests and arable land to acacia tree-dominated plantation forestry for land improvement and economic gains in Central Vietnam (Pham et al., 2023), and (ii) the reforestation program (two billion hectares reforestation, Prime Minister's Decision 147/2007/QD-TTg) in an effort to reduce natural forest degradation and enhance carbon storage between 2007 and 2015 in the central region of Vietnam invoked the conversion of degraded natural forests to planted forests (Paudyal et al., 2020; Šálek and Výlupek, 2012). Besides, the conversion from cropland to settlements and other land (5483.05 and 2762.35 ha) represented another major LULC change pattern in the research site. The observed changes were largely driven by the largescale encroachment of agricultural land to accommodate

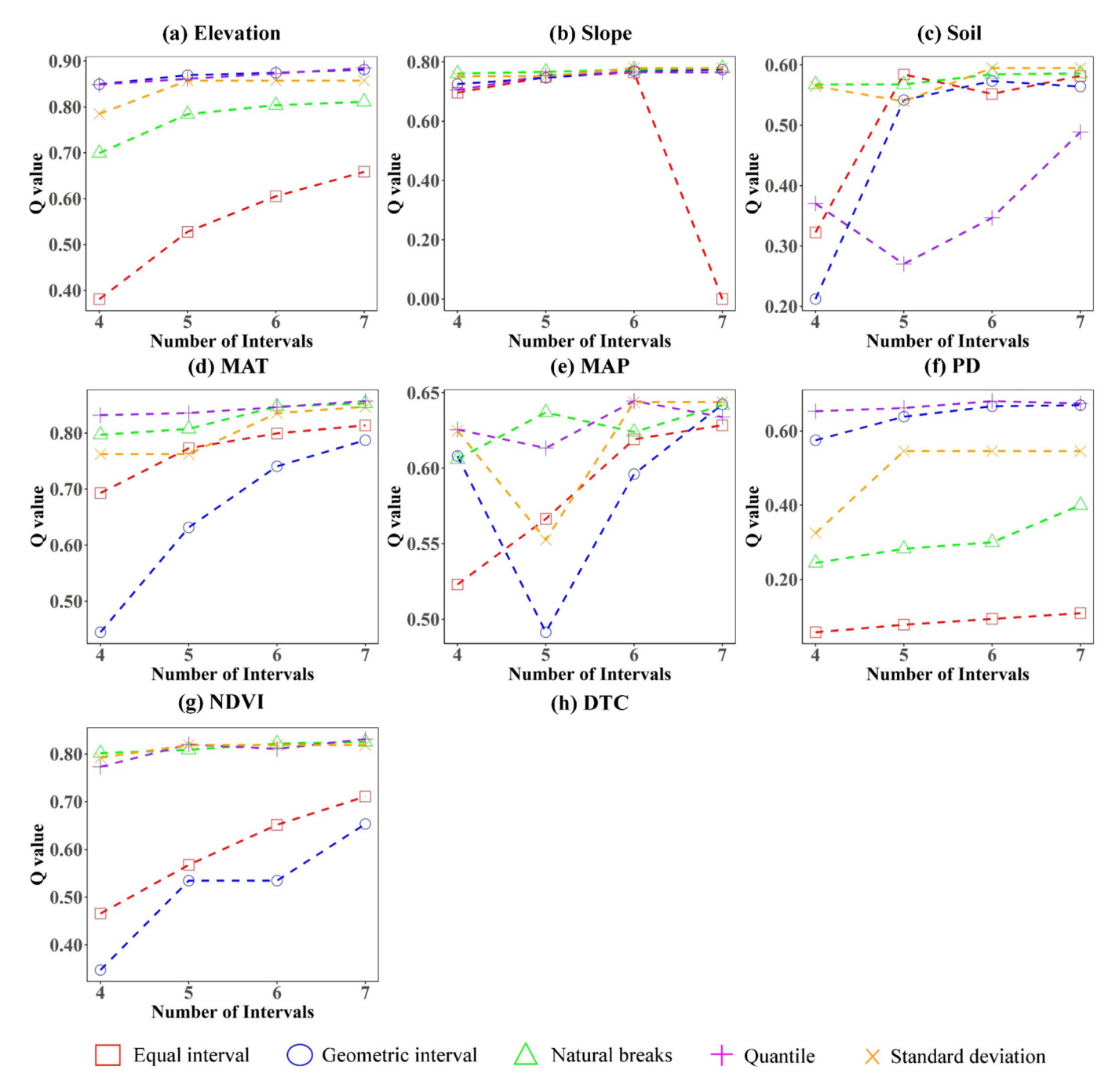


Fig. 11. Spatial data discretization for driving variables.

urban expansion and industrial development, reflecting the broader trajectory of urbanization and industrialization in Danang city (Tuan, 2021).

# 4.2. Carbon storage evolution under multiple LULC change scenarios

The SVM-CA-Markov model and the InVEST model were employed to assess the impact of LULC change imposed on the storage of carbon in Danang city in four scenarios (NTS, EPS, EDS, and CPS) from 2023 to 2050.

Generally, under these simulated scenarios, the area of plantation forest, settlements, and wetlands, along with their respective carbon storage, will increase, while those of the remaining LULC types will decrease (Fig. 7 and Table 7). Additionally, these changes in carbon storage will mostly occur in the mid-elevation regions of Danang city's central and lower areas (Fig. 8).

On the one hand, the simulated spatial distribution of LULC types and associated carbon storage projections for the next 27 years indicates that carbon storage in the region of interest is inclined to decrease under NTS,

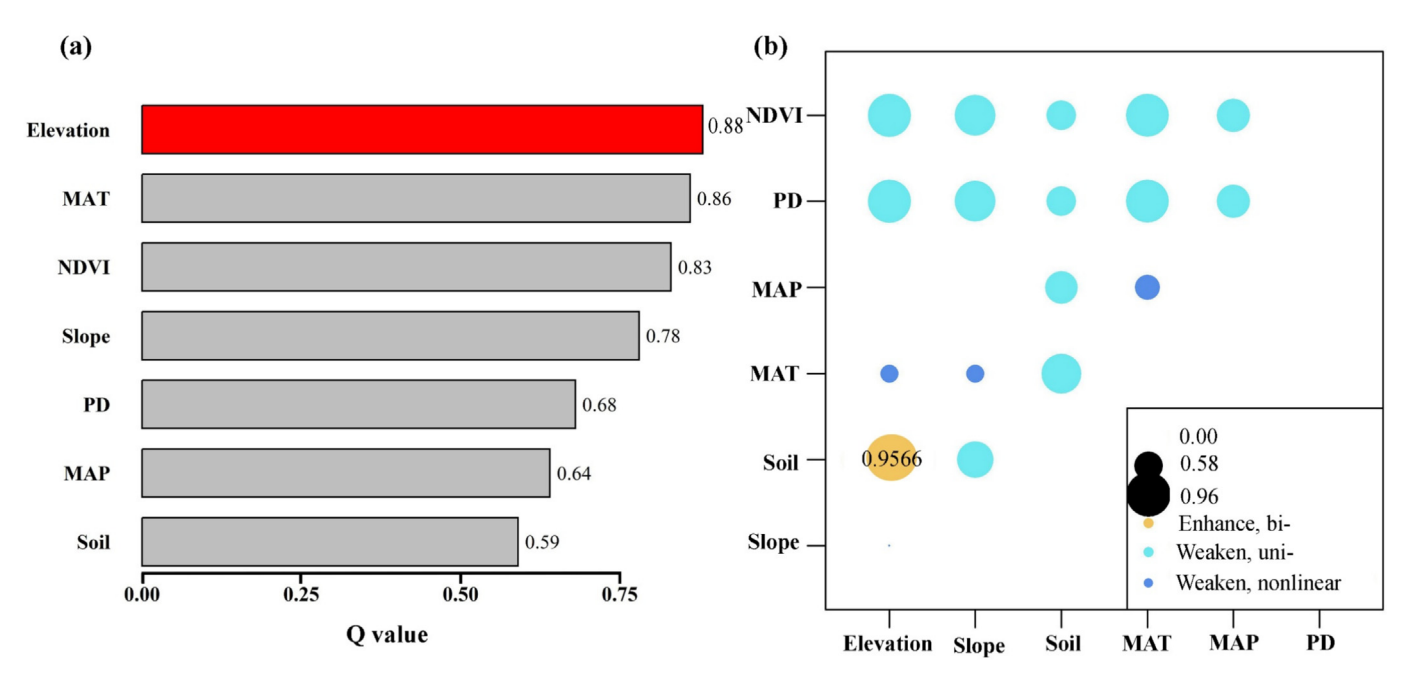


Fig. 12. Result of factor detector (a) and interaction detector (b). *Enhance, bi-*: combined effect is stronger than the sum of individual effects; *Weaken, Uni-*: Combined effect is between the strongest and weakest factor; and *Weaken, Non-linear*: Combined effect is weaker than both individual factors.

EDS, and CPS. Under NTS, given the influences of LULC change ratios and driving forces from the historical period, anthropogenic LULC changes are anticipated to drive a transition from high-carbon-density ecosystems to lowcarbon-density environments, such as the transition from natural forest to plantation forest and from cropland to settlements. Consequently, this shift will be responsible for carbon storage reduction in the study area in the absence of policy-based planning constraints. This result is conformable to previous studies which also took place in coastal areas. For example, Zhu et al. (2022) investigated the influence of LULC change on ecosystem carbon storage in Chinese coastal areas and discovered that a persistently accelerated urbanization process would result in a declining trend in carbon storage from 2020 to 2050. Zheng and Zheng (2023)'s research on coastal regions of Shandong Province (China) projected a noticeable decline in carbon storage from 2020 to 2030, attributing it to the expansion of built-up land and the corresponding reduction in cropland and forest area, without considering any further interventions. Notably, EDS possesses a trend and pace of carbon storage variation in Danang city from 2023 to 2050 that is forecast to be relatively consistent with NTS, revealing that augmenting the transition from other LULC categories to settlements for economic development orientation will not significantly modify the inherent decreasing trend of carbon storage. This finding is inconsistent with other scholars' conclusions (Li et al., 2023; Zhu et al., 2023). Of the three scenarios with declining carbon storage, the CPS will exhibit the most significant loss in carbon storage in the next nearly three decades, stemming from the transition from cultivated lands to acacia plantation forestry at a crawl. This finding is not in accord with

most previous studies in the literature. For instance, Zhu et al. (2023) promulgated that if strict adherences are taken to protect arable land, the projected reduction in carbon storage would be only half of that predicted under an urban development scenario. Lei et al. (2024) also confirmed that although the CPS would scale down the carbon storage in Hainan Island from 2020 to 2050, the pace of the downward trend would be less pronounced than under the natural development scenario. The strongest carbon storage reduction driven by CPS in our study indicates that limiting the controlled conversion of cropland to other LULC classes can adversely impact carbon storage, although descending the pressure on Danang city's food security. Thus, instead of imposing restrictions on arbitrary conversion in arable land in the context of accelerated urbanization and industrialization in the study area, alternative solutions such as agricultural intensification, agricultural specialization, market liberalization, and technical innovations should be taken into consideration to boost productivity (Huyen and Giang, 2024), while concurrently still lower reduction of carbon storage through the changeover of ineffective cropland to plantation forestry.

On the other hand, the carbon storage is prone to expand under EPS due to the constraints in refraining from encroachment on forest land by other LULC categories. In other words, the implementation of ecological protection policies is observed to be favorable for constraining the conversion of high-carbon density LULC types to low-carbon density LULC types, fostering the stable development of LULC types with high carbon sequestration capacity and augmenting the overall carbon storage capacity in Danang city. The result is consistent with the findings of Yan et al. (2024), Zhu et al. (2023), Yang et al. (2024),

and Lei et al. (2024), who reported that the scenario with ecological conservation policies will be able to either escalate or mitigate the substantial dwindling in carbon storage under the scenario of without any ecological conservation policies. The study results reveal that EPS, with its possibility of facilitating carbon sequestration, can partially contribute to realizing the country's commitment to achieving the net-zero carbon emission target by 2050 through carbon neutrality with removals from LULC change, and forestry, which is heralded in the Vietnamese Prime Minister's Decision No.896/OD-TTg.

# 4.3. Driving factors of spatial distribution of carbon storage

Relevant research indicates that the spatial distribution of carbon storage in terrestrial ecosystems is influenced by a combination of natural and anthropogenic factors, including topography, climate conditions, and vegetation characteristics (Lei et al., 2024; C. Wang et al., 2022; Yan et al., 2024). However, the possible carbon storage-driven factors are likely to be locally unique, leading to variations in the relationships between carbon storage and its driving variables across different geographical regions (Fryer and Williams, 2021; Nie et al., 2024; Pereira et al., 2015). Our study identified that the driving factors used in OPGD model analysis (including elevation, slope, soil, MAT, MAP, PD, and NDVI) had a strong impact on the spatial distribution of carbon storage, with each factor's O value surpassing 0.5 (p-values < 0.05, Fig. 12a). Among these, elevation and MAT were the most influential on the distribution characteristics of carbon storage in Danang city, with Q values achieving 0.88 and 0.86, respectively. According to the literature, higher elevations generally harbor more diverse and dense vegetation due to cooler temperatures and distinct microclimates, which facilitate greater biomass accumulation and carbon sequestration. Furthermore, these areas are often less accessible and thus less impacted by deforestation and other human activities, enabling natural vegetation to flourish (Li et al., 2023; Nie et al., 2024). This is the reason why Danang city exhibits a pattern of carbon storage that was highly in line with the distribution characteristics of elevation and MAT. Specifically, high carbon storage values were concentrated in the Ba Na – Nui Chua Nature Reserve situated in the western high-altitude mountainous regions, characterized by low temperatures and dominated by evergreen tropical vegetation. In contrast, low carbon storage values were primarily distributed in the eastern areas with lower elevations and higher temperatures, predominantly encompassing cropland and settlements. The powerful impact of elevation on ecosystem carbon storage conforms to the conclusions of previous studies. Lei et al. (2024) proclaimed that elevation, along with LULC intensity and slope, was the major factor influencing the spatial variability of carbon storage on Hainan Island, China. Similarly, Nie et al. (2024) in the research about providing insights into the direction and intensity effects of independent variables on carbon

storage distribution in Fujian Province (China) claimed that factors such as elevation, slope, and annual precipitation were identified as the most influential variables governing the spatial and temporal variation in carbon storage distribution within Fujian Province, with each factor accounting for over 50 % of the explanatory power. Regarding MAT, its strong influence on the spatial distribution of ecosystem carbon storage as in our study's finding is consistent with Xu et al. (2018), who affirmed that MAT exerted obvious impacts on the spatial patterns of carbon storage in China's terrestrial ecosystems. Whereas, Lei et al. (2024), Yan et al. (2024), and Nie et al. (2024) had an opposite perspective when they argued that MAT was the minor factor for the spatial variance of carbon storage.

Similar to the findings of previous studies (Lei et al., 2024; C. Wang et al., 2022; Yan et al., 2024), our study's interaction detection results indicate that the combined impact of two driving factors could surpass the effect of a single factor in spatially differentiating carbon storage. Among all pairwise interactions of seven factors, only the combination of elevation and soil had a synergistic enhancement effect on the spatial partitioning of carbon storage in the study site.

### 5. Conclusion

The study employed the SVM-CA-Markov model to simulate LULC dynamics in Danang city, considering four scenarios, including NTS, EPS, EDS, and CPS. The InVEST model was subsequently utilized to analyze the spatiotemporal patterns of carbon storage evolution. Finally, the driving factors of the spatial differentiation of carbon storage were evaluated by using the OPGD model. The following conclusions were obtained:

- (i) During the period from 2007 to 2023, Danang city witnessed a substantially mutual transformation between LULC types, with the transitions from natural forest to plantation forest, and from cropland to settlements, plantation forest, and other land being predominant.
- (ii) Compared with 2023, the carbon storage of Danang city in 2050 will shrink by 0.221 Mt, 0.223 Mt, and 0.298 Mt under NTS, EDS, and CPS, respectively, while enhancing by 0.141 Mt under EPS. Spatially, the higher-elevation mountainous regions in the west are projected to have the greatest carbon storage values, whereas the lower-lying eastern areas are expected to exhibit the lowest values.
- (iii) Elevation and MAT were identified as the most influential individual factors driving the spatial distribution of carbon storage. However, the interaction between elevation and soil properties exhibited a mutually reinforcing effect.

The findings of this study demonstrate the potential of integrating the SVM-CA-Markov and InVEST models as

a robust framework for simulating the evolution of ecosystem carbon storage under the influence of LULC dynamics. Practically, the scenario-based projections of carbon storage presented in this study offer valuable support for local authorities and urban planners in making informed LULC decisions that balance socioeconomic development with ecological conservation. Furthermore, the study provides a scientific foundation for national policymakers to develop tailored strategies that promote sustainable development and enhance carbon sequestration in Vietnam's Central Coastal region, thereby contributing to the achievement of national carbon neutrality commitments.

Although the linked SVM-CA-Markov and InVEST models effectively simulate the impacts of LULC change on ecosystem carbon storage, several key limitations should be acknowledged. First, the SVM-CA-Markov model does not explicitly account for planning and policy interventions in simulating past LULC transitions and spatial neighborhood rules, even though regional LULC patterns are also shaped by local policies and governance structures (Yan et al., 2024). This drawback may reduce the realism and predictive accuracy of LULC simulations in policy-sensitive regions like Danang city. Second, the InVEST model is primarily designed for large-scale assessments and focuses on differences in carbon density between LULC types, while overlooking key ecological processes such as vegetation age, photosynthetic capacity, and microbial activity (Li et al., 2023; K. Wang et al., 2022). These processes significantly influence carbon sequestration potential over time, and their omission may compromise the accuracy of long-term carbon storage estimates. To address these limitations, future research should determine how institutional and policy-related drivers can be incorporated into the LCM to improve the comprehensiveness and realism of LULC simulations. Additionally, the integration of dynamic carbon models that account for vegetation succession and ecosystem processes would improve the temporal and spatial accuracy of carbon storage estimates in the InVEST model.

# Data availability

The data supporting the findings of this study are available from the corresponding author upon reasonable request.

# Declaration of competing interest

The authors declare that they have no known competing financial interests or personal relationships that could have appeared to influence the work reported in this paper.

## Acknowledgements

We sincerely thank the Danang Department of Forest Protection for providing the necessary data and support for this research. We also extend our gratitude to our colleagues for their valuable assistance with data collection. Special thanks to Prof. Dr. Morihiro Maeda and Prof. Dr. Kazuto Shima for providing us with the needed instruments and using their laboratories at Okayama University, Japan.

### References

- Anselin, L., 1995. Local indicators of spatial association—LISA. Geogr. Anal. 27, 93–115. https://doi.org/10.1111/j.1538-4632.1995.tb00338.x.
- Avitabile, V., Schultz, M., Herold, N., de Bruin, S., Pratihast, A.K., Manh, C.P., Quang, H.V., Herold, M., 2016. Carbon emissions from land cover change in Central Vietnam. Carbon Manag. 7, 333–346. https://doi.org/10.1080/17583004.2016.1254009.
- Bacani, V.M., Machado da Silva, B.H., de Souza, A., Amede Sato, A., Souza Sampaio, B.D., Rodrigues da Cunha, E., Pereira Vick, E., Ribeiro de Oliveira, V.F., Decco, H.F., 2024. Carbon storage and sequestration in a eucalyptus productive zone in the Brazilian Cerrado, using the Ca-Markov/Random Forest and InVEST models. J. Clean. Prod. 444. https://doi.org/10.1016/j.jclepro.2024.141291 141291.
- Cairns, M.A., Brown, S., Helmer, E.H., Baumgardner, G.A., 1997. Root biomass allocation in the world's upland forests. Oecologia 111, 1–11. https://doi.org/10.1007/s004420050201.
- Cervantes, J., Garcia-Lamont, F., Rodríguez-Mazahua, L., Lopez, A., 2020. A comprehensive survey on support vector machine classification: applications, challenges and trends. Neurocomputing 408, 189– 215. https://doi.org/10.1016/j.neucom.2019.10.118.
- Cochard, R., Ngo, D.T., Waeber, P.O., Kull, C.A., 2017. Extent and causes of forest cover changes in Vietnam's provinces 1993-2013: a review and analysis of official data. Environ. Rev. 25, 199–217. https://doi.org/10.1139/er-2016-0050.
- Cochard, R., Nguyen, V.H.T., Ngo, D.T., Kull, C.A., 2020. Vietnam's forest cover changes 2005–2016: Veering from transition to (yet more) transaction?. World Dev. 135, 105051. https://doi.org/10.1016/ j.worlddev.2020.105051.
- Corbera, E., Estrada, M., Brown, K., 2010. Reducing greenhouse gas emissions from deforestation and forest degradation in developing countries: revisiting the assumptions. Clim. Change 100, 355–388. https://doi.org/10.1007/s10584-009-9773-1.
- Deng, L., Liu, S., Kim, D.G., Peng, C., Sweeney, S., Shangguan, Z., 2017.
  Past and future carbon sequestration benefits of China's grain for green program. Glob. Environ. Chang. 47, 13–20. https://doi.org/10.1016/j.gloenvcha.2017.09.006.
- Dezhkam, S., Jabbarian Amiri, B., Darvishsefat, A.A., Sakieh, Y., 2016. Performance evaluation of land change simulation models using landscape metrics. Geocarto Int. 32, 1–23. https://doi.org/10.1080/10106049.2016.1167967.
- Dondini, M., Martin, M., De Camillis, C., Uwizeye, A., Soussana, J.-F., Robinson, T., Steinfeld, H., 2023. Global assessment of soil carbon in grasslands. FAO, Rome. https://doi.org/10.4060/cc3981en.
- Friedlingstein, P., O'Sullivan, M., Jones, M.W., Andrew, R.M., Bakker, D.C.E., Hauck, J., Landschützer, P., Le Quéré, C., Luijkx, I.T., Peters, G.P., Peters, W., Pongratz, J., Schwingshackl, C., Sitch, S., Canadell, J.G., Ciais, P., Jackson, R.B., Alin, S.R., Anthoni, P., Barbero, L., Bates, N.R., Becker, M., Bellouin, N., Decharme, B., Bopp, L., Brasika, I.B.M., Cadule, P., Chamberlain, M.A., Chandra, N., Chau, T.-T.-T., Chevallier, F., Chini, L.P., Cronin, M., Dou, X., Enyo, K., Evans, W., Falk, S., Feely, R.A., Feng, L., Ford, D.J., Gasser, T., Ghattas, J., Gkritzalis, T., Grassi, G., Gregor, L., Gruber, N., Gürses, Ö., Harris, I., Hefner, M., Heinke, J., Houghton, R.A., Hurtt, G.C., Iida, Y., Ilyina, T., Jacobson, A.R., Jain, A., Jarníková, T., Jersild, A., Jiang, F., Jin, Z., Joos, F., Kato, E., Keeling, R.F., Kennedy, D., Klein Goldewijk, K., Knauer, J., Korsbakken, J.I., Körtzinger, A., Lan, X., Lefèvre, N., Li, H., Liu, J., Liu, Z., Ma, L., Marland, G., Mayot, N., McGuire, P.C., McKinley, G.A., Meyer, G., Morgan, E.J., Munro, D. R., Nakaoka, S.-I., Niwa, Y., O'Brien, K.M., Olsen, A., Omar, A.M.,

- Ono, T., Paulsen, M., Pierrot, D., Pocock, K., Poulter, B., Powis, C. M., Rehder, G., Resplandy, L., Robertson, E., Rödenbeck, C., Rosan, T.M., Schwinger, J., Séférian, R., Smallman, T.L., Smith, S.M., Sospedra-Alfonso, R., Sun, Q., Sutton, A.J., Sweeney, C., Takao, S., Tans, P.P., Tian, H., Tilbrook, B., Tsujino, H., Tubiello, F., van der Werf, G.R., van Ooijen, E., Wanninkhof, R., Watanabe, M., Wimart-Rousseau, C., Yang, D., Yang, X., Yuan, W., Yue, X., Zaehle, S., Zeng, J., Zheng, B., 2023. Global carbon budget 2023. Earth Syst. Sci. Data 15, 5301–5369. https://doi.org/10.5194/essd-15-5301-2023.
- Fryer, J., Williams, I.D., 2021. Regional carbon stock assessment and the potential effects of land cover change. Sci. Total Environ. 775. https:// doi.org/10.1016/j.scitotenv.2021.145815 145815.
- García-Ontiyuelo, M., Acuña-Alonso, C., Valero, E., Álvarez, X., 2024. Geospatial mapping of carbon estimates for forested areas using the InVEST model and Sentinel-2: a case study in Galicia (NW Spain). Sci. Total Environ. 922. https://doi.org/10.1016/j.scitotenv.2024.171297.
- Gharaibeh, A., Shaamala, A., Obeidat, R., Al-Kofahi, S., 2020. Improving land-use change modeling by integrating ANN with cellular automata-markov chain model. Heliyon 6, e05092. https://doi.org/10.1016/j.heliyon.2020.e05092.
- Ghosh, P., Mukhopadhyay, A., Chanda, A., Mondal, P., Akhand, A., Mukherjee, S., Nayak, S.K., Ghosh, S., Mitra, D., Ghosh, T., Hazra, S., 2017. Application of cellular automata and Markov-chain model in geospatial environmental modeling- a review. Remote Sens. Appl.: Soc. Environ. 5, 64–77. https://doi.org/10.1016/j.rsase.2017.01.005.
- Guan, D., Li, H., Inohae, T., Su, W., Nagaie, T., Hokao, K., 2011. Modeling urban land use change by the integration of cellular automaton and Markov model. Ecol. Modell. 222, 3761–3772. https://doi.org/10.1016/j.ecolmodel.2011.09.009.
- Ho, V.H., Morita, H., Bachofer, F., Ho, T.H., 2024. Random forest regression kriging modeling for soil organic carbon density estimation using multi-source environmental data in central Vietnamese forests. Model. Earth Syst. Environ. https://doi.org/10.1007/s40808-024-02158-1.
- Hoang Khanh Linh, N., Van Chuong, H., 2015. Assessing the impact of urbanization on urban climate by remote satellite perspective: a case study in Danang city, Vietnam. Int. Arch. Photogramm. Remote Sens. Spat. Inf. Sci. XL-7/W3, 207–212. https://doi.org/10.5194/isprsarchives-XL-7-W3-207-2015.
- Houghton, R.A., 2018. Interactions between land-use change and climatecarbon cycle feedbacks. Curr. Clim. Chang. Reports 4, 115–127. https://doi.org/10.1007/s40641-018-0099-9.
- Houghton, R.A., House, J.I., Pongratz, J., van der Werf, G.R., DeFries, R.S., Hansen, M.C., Le Quéré, C., Ramankutty, N., 2012. Carbon emissions from land use and land-cover change. Biogeosciences 9, 5125–5142. https://doi.org/10.5194/bg-9-5125-2012.
- Huang, S., Ghazali, S., Azadi, H., Movahhed Moghaddam, S., Viira, A.-H., Janečková, K., Sklenička, P., Lopez-Carr, D., Köhl, M., Kurban, A., 2023. Contribution of agricultural land conversion to global GHG emissions: a meta-analysis. Sci. Total Environ. 876. https://doi.org/ 10.1016/j.scitotenv.2023.162269 162269.
- Huy, B., Poudel, K.P., Temesgen, H., 2016. Aboveground biomass equations for evergreen broadleaf forests in South Central Coastal ecoregion of Viet Nam: selection of eco-regional or pantropical models. For. Ecol. Manage. 376, 276–283. https://doi.org/10.1016/ j.foreco.2016.06.031.
- Huyen, P.T.T., Giang, P.Q., 2024. Agricultural land use in Vietnam in the context of urbanization: status and policy implications. Environ. Socio-Economic Stud. 12, 51–62. https://doi.org/10.2478/environ-2024-0005.
- IPCC, 2006. 2006 IPCC guidelines for national greenhouse gas inventories, Prepared by the National Greenhouse Gas Inventories Programme, Eggleston H.S., Buendia L., Miwa K., Ngara T. and Tanabe K. (Eds.), Japan.
- Ismail, I., Gaganis, V., 2024. Well Control Strategies for Effective CO2 Subsurface Storage: Optimization and Policies, in: RawMat 2023. MDPI, Basel Switzerland, p. 74. https://doi.org/10. 3390/materproc2023015074.

- Jiang, F., Sun, H., Chen, E., Wang, T., Cao, Y., Liu, Q., 2022. Above-ground biomass estimation for coniferous forests in northern china using regression kriging and landsat 9 images. Remote Sens. 14, 5734. https://doi.org/10.3390/rs14225734.
- Kim, O.S., 2010. An assessment of deforestation models for reducing emissions from deforestation and forest degradation (REDD). Trans. GIS 14, 631–654. https://doi.org/10.1111/j.1467-9671.2010.01227.x.
- Kissinger, G., Brockhaus, M., Bush, S.R., 2021. Policy integration as a means to address policy fragmentation: assessing the role of Vietnam's national REDD+ action plan in the central highlands. Environ. Sci. Policy 119, 85–92. https://doi.org/10.1016/j.envsci.2021.02.011.
- Kura, A.L., Beyene, D.L., 2020. Cellular automata Markov chain model based deforestation modelling in the pastoral and agro-pastoral areas of southern Ethiopia. Remote Sens. Appl.: Soc. Environ. 18. https:// doi.org/10.1016/j.rsase.2020.100321 100321.
- Lei, J., Zhang, L., Chen, Z., Wu, T., Chen, X., Li, Y., 2024. The impact of land use change on carbon storage and multi-scenario prediction in Hainan Island using InVEST and CA-Markov models. Front. Glob. Chang. 7, 1–17. https://doi.org/10.3389/ffgc.2024.1349057.
- Li, P., Chen, J., Li, Y., Wu, W., 2023. Using the InVEST-PLUS model to predict and analyze the pattern of ecosystem carbon storage in Liaoning Province. China. Remote Sens. 15, 4050. https://doi.org/ 10.3390/rs15164050.
- Liang, Y., Zeng, J., Li, S., 2022. Examining the spatial variations of land use change and its impact factors in a coastal area in Vietnam. Land 11, 1751. https://doi.org/10.3390/land11101751.
- M., K., Linh, N.H.K., Kappas, M., Hoang, N., Linh, K., M., K., Linh, N. H.K., 2012. Spatio-temporal dynamics and evolution of landscape pattern in coastal areas of central region, Vietnam. VNU J. Sci. Earth Environ. Sci. 28, 251–263.
- Marko, K., Zulkarnain, F., Kusratmoko, E., 2016. Coupling of Markov chains and cellular automata spatial models to predict land cover changes (case study: upper Ci Leungsi catchment area). IOP Conf. Ser.: Earth Environ. Sci 47. https://doi.org/10.1088/1755-1315/47/1/ 012032 012032.
- Mauya, E.W., Mugasha, W.A., Njana, M.A., Zahabu, E., Malimbwi, R., 2019. Carbon stocks for different land cover types in Mainland Tanzania. Carbon Balance Manag. 14, 4. https://doi.org/10.1186/ s13021-019-0120-1.
- McRoberts, R.E., Tomppo, E.O., Czaplewski, R.L., 2015. Sampling designs for national forest assessments. Knowl. Ref. Natl. for. Assessments, 23–40.
- Munthali, M.G., Mustak, S., Adeola, A., Botai, J., Singh, S.K., Davis, N., 2020. Modelling land use and land cover dynamics of Dedza district of Malawi using hybrid Cellular Automata and Markov model. Remote Sens. Appl.: Soc. Environ. 17, 100276. https://doi.org/10.1016/j.rsase.2019.100276.
- Mustafa, A., Rienow, A., Saadi, I., Cools, M., Teller, J., 2018. Comparing support vector machines with logistic regression for calibrating cellular automata land use change models. Eur. J. Remote Sens. 51, 391–401. https://doi.org/10.1080/22797254.2018.1442179.
- Nayak, S., Mandal, M., 2019. Impact of land use and land cover changes on temperature trends over India. Land Use Policy 89, 104238. https:// doi.org/10.1016/j.landusepol.2019.104238.
- Nie, Q., Wu, G., Li, L., Man, W., Ma, J., Bao, Z., Luo, L., Li, H., 2024. Exploring scaling differences and spatial heterogeneity in drivers of carbon storage changes: a comprehensive geographic analysis framework. Ecol. Indic. 165, 112193. https://doi.org/10.1016/j. ecolind 2024 112193
- Nilsson, S., Schopfhauser, W., 1995. The carbon-sequestration potential of a global afforestation program. Clim. Change 30, 267–293. https:// doi.org/10.1007/BF01091928.
- Nyamekye, C., Kwofie, S., Agyapong, E., Ofosu, S.A., Arthur, R., Appiah, L.B., 2021. Integrating support vector machine and cellular automata for modelling land cover change in the tropical rainforest under equatorial climate in Ghana. Curr. Res. Environ. Sustain. 3, 100052. https://doi.org/10.1016/j.crsust.2021.100052.

- Olorunfemi, I.E., Fasinmirin, J.T., Olufayo, A.A., Komolafe, A.A., 2020. Total carbon and nitrogen stocks under different land use/land cover types in the Southwestern region of Nigeria. Geoderma Reg. 22, e00320. https://doi.org/10.1016/j.geodrs.2020.e00320.
- Omar, N.Q., Ahamad, M.S.S., Wan Hussin, W.M.A., Samat, N., Binti Ahmad, S.Z., 2014. Markov CA, multi regression, and multiple decision making for modeling historical changes in Kirkuk City. Iraq. J. Indian Soc. Remote Sens. 42, 165–178. https://doi.org/10.1007/ s12524-013-0311-2.
- Paudyal, K., Samsudin, Y.B., Baral, H., Okarda, B., Phuong, V.T., Paudel, S., Keenan, R.J., 2020. Spatial assessment of ecosystem services from planted forests in Central Vietnam. Forests 11, 822. https://doi.org/10.3390/f11080822.
- Pearson, T.R.H., Brown, S.L., Birdsey, R.A., 2007. Measurement guidelines for the sequestration of forest carbon. U.S. Department of Agriculture, Forest Service, Northern Research Station. https://doi. org/10.2737/NRS-GTR-18.
- Pereira, O.J.R., Montes, C.R., Lucas, Y., Santin, R.C., Melfi, A.J., 2015. A multi-sensor approach for mapping plant-derived carbon storage in amazonian podzols. Int. J. Remote Sens. 36, 2076–2092. https://doi. org/10.1080/01431161.2015.1034896.
- Pham, T.P.T., Tran, N.T., Kull, C.A., Shackleton, R.T., Cochard, R., Nguyen, T.H.M., Ngo, T.D., Nguyen, T.H.V., Tran, Q.C., Vu, T.T.T., 2023. Factors influencing farmers' forestland-use changes over 15 years (2005–2020) in Thua Thien Hue province. Vietnam. Int. for. Rev. 25, 71–91. https://doi.org/10.1505/146554823836838682.
- Phuong, N.C., Richard, J., 2011. Economic transition and accounting system reform in Vietnam. Eur. Account. Rev. 20, 693–725. https:// doi.org/10.1080/09638180.2011.623858.
- Pielke, R.A., Pitman, A., Niyogi, D., Mahmood, R., McAlpine, C., Hossain, F., Goldewijk, K.K., Nair, U., Betts, R., Fall, S., Reichstein, M., Kabat, P., de Noblet, N., 2011. Land use/land cover changes and climate: modeling analysis and observational evidence. Wiley Interdiscip. Rev. Clim. Chang. 2, 828–850. https://doi.org/10.1002/wcc.144.
- Pontius, R.G., Millones, M., 2011. Death to Kappa: birth of quantity disagreement and allocation disagreement for accuracy assessment. Int. J. Remote Sens. 32, 4407–4429. https://doi.org/10.1080/ 01431161.2011.552923.
- Šálek, L., Výlupek, O., 2012. Contribution to the Restoration of mixed forests in Central Vietnam. J. Sustain. For. 31, 549–562. https://doi.org/10.1080/10549811.2011.648525.
- Schulp, C.J.E., Nabuurs, G.-J., Verburg, P.H., 2008. Future carbon sequestration in Europe—Effects of land use change. Agric. Ecosyst. Environ. 127, 251–264. https://doi.org/10.1016/j.agee.2008.04.010.
- Singh, S.K., Thawale, P.R., Sharma, J.K., Gautam, R.K., Kundargi, G. P., Juwarkar, A.A., 2015. In: Carbon Sequestration in Terrestrial Ecosystems. Springer International Publishing, Cham, pp. 99–131. https://doi.org/10.1007/978-3-319-19375-5\_3.
- Solaimani, K., Darvishi, S., 2024. Comparative analysis of land use changes modeling based-on new hybrid models and CA-Markov in the Urmia lake basin. Adv. Sp. Res. 74, 3749–3764. https://doi.org/ 10.1016/j.asr.2024.06.078.
- Song, Y., Wang, J., Ge, Y., Xu, C., 2020. An optimal parameters-based geographical detector model enhances geographic characteristics of explanatory variables for spatial heterogeneity analysis: cases with different types of spatial data. Giscience Remote Sens. 57, 593–610. https://doi.org/10.1080/15481603.2020.1760434.
- Subedi, P., Subedi, K., Thapa, B., 2013. Application of a hybrid cellular automaton – Markov (CA-Markov) model in land-use change prediction: a case study of saddle creek drainage basin, Florida. Appl. Ecol. Environ. Sci. 1, 126–132. https://doi.org/10.12691/aees-1-6-5.
- Sun, M., 2014. Support Vector Machine Models for Classification, in: Encyclopedia of Business Analytics and Optimization. IGI Global, pp. 2395–2409. https://doi.org/10.4018/978-1-4666-5202-6.ch215.
- Tuan, N.T., 2022. Urbanization and land use change: a study in Vietnam. Environ. Socio-Economic Stud. 10, 19–29. https://doi.org/10.2478/environ-2022-0008.

- Tuan, N.T., 2021. The consequences of expropriation of agricultural land and loss of livelihoods on those households who lost land in Da Nang, Vietnam. Environ. Socio-Economic Stud. 9, 26–38. https://doi.org/ 10.2478/environ-2021-0008.
- Ussiri, D.A.N., Lal, R., 2017. Carbon Sequestration for Climate Change Mitigation and Adaptation, Mass Communication and Society. Springer International Publishing, Cham. https://doi.org/10.1007/978-3-319-53845-7.
- V.H., Trieu, T.T., P., L.C., D.T., 2020. Vietnam Forestry Development Strategy: Implementation results for 2006–2020 and recommendations for the 2021–2030 strategy. Center for International Forestry Research (CIFOR). https://doi.org/10.17528/cifor/007879.
- Verma, P., Siddiqui, A.R., Mourya, N.K., Devi, A.R., 2024. Forest carbon sequestration mapping and economic quantification infusing MLPnn-Markov chain and InVEST carbon model in Askot Wildlife Sanctuary, Western Himalaya. Ecol. Inform. 79, 102428. https://doi. org/10.1016/j.ecoinf.2023.102428.
- Wang, C., Luo, J., Qing, F., Tang, Y., Wang, Y., 2022a. Analysis of the driving force of spatial and temporal differentiation of carbon storage in taihang mountains based on InVEST model. Appl. Sci. 12, 10662. https://doi.org/10.3390/app122010662.
- Wang, K., Li, X., Lyu, X., Dang, D., Dou, H., Li, M., Liu, S., Cao, W., 2022b. Optimizing the land use and land cover pattern to increase its contribution to carbon neutrality. Remote Sens. 14, 4751. https://doi. org/10.3390/rs14194751.
- Xu, L., Yu, G., He, N., Wang, Q., Gao, Y., Wen, D., Li, S., Niu, S., Ge, J., 2018. Carbon storage in China's terrestrial ecosystems: a synthesis. Sci. Rep. 8, 2806. https://doi.org/10.1038/s41598-018-20764-9.
- Yan, X., Li, M., Guo, D., Yang, D., Zhan, D., 2024. Spatial-temporal evolution and prediction of carbon storage in Mohe city by linking the logistic-CA-Markov and InVEST models. Front. Earth Sci. 12, 1–19. https://doi.org/10.3389/feart.2024.1383237.
- Yang, Q., Li, X., Shi, X., 2008. Cellular automata for simulating land use changes based on support vector machines. Comput. Geosci. 34, 592– 602. https://doi.org/10.1016/j.cageo.2007.08.003.
- Yang, S., Li, L., Zhu, R., Luo, C., Lu, X., Sun, M., Xu, B., 2024. Assessing land-use changes and carbon storage: a case study of the Jialing River Basin, China. Sci. Rep. 14, 15984. https://doi.org/ 10.1038/s41598-024-66742-2.
- Zhang, L., Li, G., Liu, S., Wang, N., Yu, D., Pan, Y., Yang, X., 2022. Spatiotemporal variations and driving factors of coastline in the Bohai Sea. J. Ocean Univ. China 21, 1517–1528. https://doi.org/10.1007/s11802-022-5114-z.
- Zhao, M., He, Z., Du, J., Chen, L., Lin, P., Fang, S., 2019. Assessing the effects of ecological engineering on carbon storage by linking the CA-Markov and InVEST models. Ecol. Indic. 98, 29–38. https://doi.org/10.1016/j.ecolind.2018.10.052.
- Zheng, H., Zheng, H., 2023. Assessment and prediction of carbon storage based on land use/land cover dynamics in the coastal area of Shandong Province. Ecol. Indic. 153, 110474. https://doi.org/10.1016/j. ecolind.2023.110474.
- Zheng, Z., Wu, Z., Chen, Y., Yang, Z., Marinello, F., 2020. Exploration of eco-environment and urbanization changes in coastal zones: a case study in China over the past 20 years. Ecol. Indic. 119, 106847. https:// doi.org/10.1016/j.ecolind.2020.106847.
- Zhi, J., Zhou, Z., Cao, X., 2021. Exploring the determinants and distribution patterns of soil mattic horizon thickness in a typical alpine environment using boosted regression trees. Ecol. Indic. 133, 108373. https://doi.org/10.1016/j.ecolind.2021.108373.
- Zhu, J., Hu, X., Xu, W., Shi, J., Huang, Y., Yan, B., 2023. Regional carbon stock response to land use structure change and multi-scenario prediction: a case study of Hunan Province. China. Sustainability 15, 12178. https://doi.org/10.3390/su151612178.
- Zhu, L., Song, R., Sun, S., Li, Y., Hu, K., 2022. Land use/land cover change and its impact on ecosystem carbon storage in coastal areas of China from 1980 to 2050. Ecol. Indic. 142, 109178. https://doi.org/ 10.1016/j.ecolind.2022.109178.